REPORT DOCUMENTATION PAGE

Form Approved
OMB No. 0704-0188

1. REPO... ...TE (DD-MM-YYYY)	2. REPORT TYPE	3. DATES COVERED (From - To)
	Technical Papers	

4. TITLE AND SUBTITLE

Please see attached

5a. CONTRACT NUMBER

5b. GRANT NUMBER

5c. PROGRAM ELEMENT NUMBER

6. AUTHOR(S)

5d. PROJECT NUMBER
5503

5e. TASK NUMBER
000P

5f. WORK UNIT NUMBER
549807

7. PERFORMING ORGANIZATION NAME(S) AND ADDRESS(ES)

Air Force Research Laboratory (AFMC)
AFRL/PRS
5 Pollux Drive
Edwards AFB CA 93524-7048

8. PERFORMING ORGANIZATION REPORT

9. SPONSORING / MONITORING AGENCY NAME(S) AND ADDRESS(ES)

Air Force Research Laboratory (AFMC)
AFRL/PRS
5 Pollux Drive
Edwards AFB CA 93524-7048

10. SPONSOR/MONITOR'S ACRONYM(S)

11. SPONSOR/MONITOR'S NUMBER(S)
Please see attached

12. DISTRIBUTION / AVAILABILITY STATEMENT

Approved for public release; distribution unlimited.

13. SUPPLEMENTARY NOTES

14. ABSTRACT

20030206 074

15. SUBJECT TERMS

16. SECURITY CLASSIFICATION OF:			17. LIMITATION OF ABSTRACT	18. NUMBER OF PAGES	19a. NAME OF RESPONSIBLE PERSON
a. REPORT	b. ABSTRACT	c. THIS PAGE			Leilani Richardson
Unclassified	Unclassified	Unclassified	A		19b. TELEPHONE NUMBER (include area code) (661) 275-5015

CP

MEMORANDUM FOR PRS (Contractor Publication)

FROM: PROI (STINFO) 14 February 2002

SUBJECT: Authorization for Release of Technical Information, Control Number: **AFRL-PR-ED-TP-2002-028**
W.H. Calhoon, Jr.; D.C. Kenzakowski (CRAFT), "Assessment of Turbulence-Chemistry Interactions in Missile Exhaust Plume Signature Analysis"

Journal of Propulsion and Power **(Statement A)**
Deadline: N/A)

1. This request has been reviewed by the Foreign Disclosure Office for: a.) appropriateness of distribution statement, b.) military/national critical technology, c.) export controls or distribution restrictions, d.) appropriateness for release to a foreign nation, and e.) technical sensitivity and/or economic sensitivity.
Comments:_____

Signature _____ Date _____

2. This request has been reviewed by the Public Affairs Office for: a.) appropriateness for public release and/or b) possible higher headquarters review.
Comments: _____

Signature _____ Date _____

3. This request has been reviewed by the STINFO for: a.) changes if approved as amended, b) appropriateness of references, if applicable; and c.) format and completion of meeting clearance form if required
Comments:_____

Signature _____ Date _____

4. This request has been reviewed by PR for: a.) technical accuracy, b.) appropriateness for audience, c.) appropriateness of distribution statement, d.) technical sensitivity and economic sensitivity, e.) military/ national critical technology, and f.) data rights and patentability
Comments:_____

APPROVED/APPROVED AS AMENDED/DISAPPROVED

_____

PHILIP A. KESSEL Date
Technical Advisor
Space and Missile Propulsion Division

ASSESSMENT OF TURBULENCE-CHEMISTRY INTERACTIONS IN MISSILE EXHAUST PLUME SIGNATURE ANALYSIS

W. H. Calhoon, Jr.†

Combustion Research and Flow Technology

Redstone Arsenal, AL

D. C. Kenzakowski‡

Combustion Research and Flow Technology

Dublin, PA

ABSTRACT

The combustion or afterburning of fuel-rich rocket exhaust with the atmosphere may result in large infrared radiation emissions which can play a significant role in the design of missile base components and missile defense systems. Current engineering level models neglect turbulence-chemistry interactions and typically underpredict the intensity of plume afterburning and afterburning burnout. To evaluate the impact of turbulence-chemistry interactions, an assumed pdf model was applied to missile plume simulations of a generic booster. Simulation results reveal turbulence-chemistry interactions to have a large impact on plume signatures as afterburning burnout was approached.

---

† Senior Research Scientist, Member AIAA
‡ Senior Research Scientist, Member AIAA.
Combustion Research and Flow Technology
US Army Aviation and Missile Command
AMSAM-RD-SS-AT
Redstone Arsenal, AL 35898-5000
Email: calhoon@cfd.rdec.redstone.army.mil

NOMENCLATURE

C_1, C_g, C_2, C_Q	=	model calibration coefficients
c_v	=	mixture specific heat at constant volume
$\hat{c}_v$	=	mean mixture specific heat neglecting turbulent fluctuations
e	=	mixture specific internal energy
e_k	=	kth species specific internal energy
$<g>$	=	specific internal energy variance
h	=	mixture specific enthalpy
k	=	turbulent kinetic energy
p	=	pressure
P	=	single-point joint probability density function (pdf) of density, temperature and species mass fraction
P_Q	=	marginal pdf of scalar energy
P_T	=	marginal pdf of temperature
P_ρ	=	marginal pdf of density
Pr	=	Prandtl number
Pr_T	=	turbulent Prandtl number
Q	=	scalar energy
R^o	=	universal gas constant
S	=	sum of the species mass fraction variance
Sc	=	Schmidt number
Sc_T	=	turbulent Schmidt number
t	=	time

T	=	temperature
T_{min}, T_{max}	=	P_T pdf minimum and maximum realizable temperatures
T_0, T_1	=	P_T pdf minimum and maximum absolute realizable temperatures
$< T''^2 >$	=	temperature variance
u_j	=	jth velocity component
$\dot{w}_k$	=	kth species reaction rate
W_k	=	kth species molecular weight
x_j	=	jth spatial coordinate
x_{refl}	=	distance between missile nozzle exit plane and the plume barrel shock reflection point at the axis of symmetry
Y_k	=	kth species mass fraction
$\beta_1, \beta_2, ..., \beta_K$	=	beta function pdf parameters
δ	=	plume transverse length scale
Δ	=	delta function
ε	=	turbulent kinetic energy dissipation rate
γ	=	ratio of mixture specific heats
Γ	=	gamma function
ν	=	kinematic viscosity
ν_T	=	turbulent eddy viscosity
ρ	=	density
θ	=	normalized temperature

Superscripts

"	=	Favre fluctuating component

Other marks

$\bar{}$	=	time-averaged quantity
$\langle\ \rangle$	=	Favre-averaged quantity

I. INTRODUCTION

The afterburning of missile exhaust with the atmosphere may result in large infrared radiation emission which can be a major contributor to the heat transfer to the missile base.[1] As altitude is increased, the radiative component of the heat transfer rate will eventually show a large drop in magnitude[2] resulting from the shutdown or cessation of afterburning in the plume (see Fig. 1). Shutdown in this context does not refer to the termination of the missile engine, but to the cessation of the combustion taking place between the missile exhaust and the atmosphere, occurring with continuous engine operation. The total amount of time this afterburning occurs and its rate of decay during the shutdown event will determine the total heat transfer to the body and establish a design criteria for the components in the base region. The radiative emission during the shutdown event also has important implications for the development of missile defense systems. Consequently, a need exists to accurately characterize missile plume afterburning shutdown or cessation events.

The character of afterburning shutdown events has been observed to vary among different propulsion systems. For example, during shutdown some systems exhibit a very rapid drop in total radiant intensity over a narrow altitude range, whereas others shutdown gradually over a wide range. The prediction of afterburning shutdown using engineering level modeling techniques[3] has been relatively successful for systems that exhibit the gradual drop-off type of shutdown event. However, these techniques have been less successful in predicting shutdown for systems that exhibit the rapid drop-off behavior.

To improve understanding into the physical mechanisms producing afterburning shutdown, Calhoon[4] investigated the shutdown characteristics of a generic amine booster system within the

framework of a computational parametric study. Several mechanisms were investigated to explain the shutdown behavior of this system which included: 1) a plume shear layer relaminarization phenomenon, 2) a Damköhler number effect and 3) a classical flame extinction mechanism. The relaminarization mechanism was found to be implausible because plume shear layer Reynolds numbers were well above transition after shutdown had occurred. The Damköhler number mechanism was found to be plausible and indeed the *only* shutdown mechanism modeled within most commercially available codes. This is a consequence of the assumptions used to model the mean reaction rate in the species conservation equations. The Damköhler number mechanism was found to be responsible for the gradual drop-off rates of plume radiation produced by most codes. The classical flame extinction mechanism was found to be a possible explanation for the observed rapid shutdown behavior of some systems.

The flame extinction phenomenon investigated by Calhoon[4] is a result of the interaction of turbulence and chemistry at small spatial scales. The model used by Calhoon[4] to account for this phenomenon was an elementary one applicable to high speed compressible flows. Other models do exist to more generally account for turbulence-chemistry interactions that are applicable to compressible flows. Among the most comprehensive techniques are the assumed probability-density-function (pdf) method[5] and the compressible extension of the pdf evolution equation method[6,7]. Though providing a more accurate description of the higher order statistics of the turbulent scalar fields, the pdf evolution equation method has not been shown to yield significantly better results than the assumed pdf method when applied to compressible flows. The pdf evolution equation method is also computationally expensive and may become intractable when applied to flows including shock waves.[7] The assumed pdf method, on the other hand, is computationally inexpensive and offers a viable approach to account for turbulence-chemistry interactions in

complex, large scale flows of practical interest. However, the assumed pdf method does not directly account for strain extinction effects and may not accurately capture this phenomenon.

For high speed flows, turbulence-chemistry interactions have been shown to enhance burning for flames far from equilibrium.[8] Including turbulence-chemistry interactions within rocket plume simulations has the potential to improve predictive capability because engineering level modeling techniques typically underpredict afterburning plume temperatures and emissions near the afterburning shutdown regime. Including turbulent fluctuations within the radiation calculations may also significantly impact predictions.[9] However, this aspect of the problem was not considered in this study. The effect of turbulent fluctuations was only considered for the flowfield predictions.

The objective of this study was to assess the impact of turbulence-chemistry interactions on the afterburning and afterburning shutdown characteristics of a generic missile system. This assessment will provide guidance for further investigation and for the enhancement of engineering level models. This work is a continuation of a previous study[4] that investigated mechanisms influencing the afterburning shutdown characteristics of rocket exhaust plumes.

In the following sections a brief review of the assumed pdf turbulence-chemistry interaction model is first given. The computational methodology used within the simulations is then presented, followed by a description of the generic missile geometry and engine model used. Results are then presented for the prediction of afterburning shutdown for this missile configuration using the assumed pdf model followed by conclusions that may be drawn from the study. These results indicate that turbulence-chemistry interactions do play a significant role in the afterburning and afterburning shutdown characteristics of missile exhaust plumes.

II. ASSUMED PDF METHOD

The effect of turbulence-chemistry interactions within the context of Reynolds averaged Navier-Stokes simulations (RANS) appears as additional unclosed terms in the governing steady

state conservation equations. These unclosed terms include: 1) the time averaged reaction rate term $\overline{\dot{w}_k}$ in the species conservation equations and 2) temperature-species correlations in the state equations. The reaction rate is a highly nonlinear function of temperature and species concentrations and its time average may be expressed as,

$$\overline{\dot{w}_k} = \int_0^\infty \int_0^\infty \int_0^1 \cdots \int_0^1 \int_0^1 \dot{w}_k(\rho, T, Y_k) P(\rho, T, Y_k) dY_1 \ldots dY_K dT d\rho \tag{1}$$

where T, ρ, Y_k and $\dot{w}_k$ are the temperature, density and kth species mass fraction and reaction rate for species $1 \le k \le K$. $P(\rho, T, Y_k)$ is the single-point joint probability density function of ρ, T and Y_k and represents the combined effects of turbulent transport, both large and small scale, and molecular diffusion. The time averaged state equation for a mixture of perfect gases may be written as,

$$\overline{p} = \overline{\rho} R^o \sum_{k=1}^{K} \frac{< T >< Y_k >}{W_k} + R^o \overline{\rho} \sum_{k=1}^{K} \frac{< T'' Y_k'' >}{W_k} \tag{2}$$

where the overbar and brackets (< >) represent conventional and Favre time averaging, respectively. Also, p is the pressure, R^o is the universal gas constant and W_k is the kth species molecular weight. The fluctuating components T'' and Y_k'' of T and Y_k are defined by $T = < T > + T''$ and $Y_k = < Y_k > + Y_k''$, respectively.

Temperature-species correlations similar to what is seen in Equ. (2) also appear in the time averaged caloric equation of state, $< h > = < e > + \overline{p} / \overline{\rho}$, relating the internal energy to enthalpy. Expressing the species specific enthalpies in terms of standard polynomial curve fits, the time averaged enthalpy becomes $< h > = f(\overline{\rho T'' Y_k''}, \ldots, \overline{\rho T''^N Y_k''})$ where N is the number of coefficients in the fits.

To close the governing flow equations, an approximation for the pdf P must be specified. Within the context of the assumed pdf approach, the shape of P is specified in terms of functions

which may be parameterized by their lower moments. The first approximation used within this approach is to assume statistical independence of ρ, T and Y_k so that P may be expressed as,

$$P(\rho,T,Y_k) = P_\rho(\rho)P_T(T)P_Q(Y_k) \tag{3}$$

where P_ρ, P_T and P_Q are the marginal pdf's of ρ, T and Y_k, respectively. This assumption is questionable. However, other assumed pdf methods cast in terms of a mixture fraction and chemical progress variable have been shown to produce good results for a range of low speed turbulent reacting flow problems using this assumption. Consequently, this assumption is carried over to the more general formulation described here. This assumption also results in $< T''Y_k'' >= 0$ in Equ. (2) since the variables are not correlated.

Baurle and Girimaji[10] investigated a modification to this procedure which relaxed the statistical independence assumption and showed potential for improvement. However, further research is required to resolve realizability issues that were identified. Therefore, this modified approach was not considered further in this study.

Consistent with work of Gaffney, *et al.*[5], the marginal pdf's P_ρ, P_T and P_Q were specified as follows. A delta function was assumed for the marginal pdf of density so that $P_\rho = \Delta(\rho - \overline{\rho})$. For the temperature pdf P_T, a beta function was used. The beta function has been shown to accurately capture scalar *mixing* in homogeneous turbulence.[11] The pdf P_T was taken as,

$$P_T(\theta) = \frac{\theta^{\beta_1-1}(1-\theta)^{\beta_2-1}}{\Gamma(\beta_1)\Gamma(\beta_2)}\Gamma(\beta_1+\beta_2) \tag{4}$$

with,

$$\begin{aligned} \beta_1 &= <\theta>\left[\frac{<\theta>(1-<\theta>)}{<\theta''\theta''>}-1\right] \\ \beta_2 &= (1-<\theta>)\left[\frac{<\theta>(1-<\theta>)}{<\theta''\theta''>}-1\right] \end{aligned} \tag{5}$$

and,

$$\theta = \frac{T - T_{\min}}{T_{\max} - T_{\min}}, \qquad <\theta> = \frac{<T> - T_{\min}}{T_{\max} - T_{\min}}$$
$$<\theta''\theta''> = \frac{<T''T''>}{(T_{\max} - T_{\min})^2} \tag{6}$$

where Γ is the gamma function. The variance $<\theta''\theta''>$ was explicitly limited by the realizability constraint,

$$<\theta''\theta''> \leq <\theta>(1 - <\theta>) \tag{7}$$

The temperature limits T_{min} and T_{max} were specified as,

$$T_{\min} = \max[T_0, <T> - n\sqrt{<T''^2>}]$$
$$T_{\max} = \min[T_1, <T> + n\sqrt{<T''^2>}] \tag{8}$$

where the coefficient n was specified to have a value of *3* following Gaffney, *et al.*[8] The values T_0 and T_1 are problem dependent absolute minimum and maximum realizable temperature limits, respectively. Specifying T_{min} and T_{max} in this manner gives the pdf a symmetric distribution for small temperature variance while allowing for nonsymmetric shapes when the limits are capped by T_0 and/or T_1. Allowing nonsymmetric pdf shapes also allows for the physically realistic situation of temperature intensities being greater than 1 (i.e., $\sqrt{<T''^2>}/<T> 1$).

For the pdf P_Q, a multivariate beta distribution was used and has the following form,

$$P_Q(Y_1, Y_2, ..., Y_K) = \frac{\Gamma(\beta_1 + \beta_2 + ... + \beta_K)}{\Gamma(\beta_1)\Gamma(\beta_2)...\Gamma(\beta_K)} Y_1^{\beta_1 - 1} Y_2^{\beta_2 - 1} ... Y_K^{\beta_K - 1} \Delta(1 - \sum_{k=1}^{K} Y_k) \tag{9}$$

with,

$$\beta_k = <Y_k> \left(\frac{1 - S}{Q} - 1 \right) \tag{10}$$

where,

$$S = \sum_{k=1}^{K} <Y_k>^2, \quad Q = \sum_{k=1}^{K} <Y_k'' Y_k''> \tag{11}$$

The quantity Q is the sum of the species variances and is called the turbulent scalar energy. As with P_T, a realizability condition must be explicitly imposed. This condition was $Q \le (1-S)$.

With Equs. (4) - (11), the joint pdf of ρ, T and Y_k is completely specified given $<T>$, $<T''T''>$, $<Y_k>$ and Q. The mean reaction rate may then be calculated from Equ. (1). Numerically integrating Equ. (1) can become very computationally expensive for a large number of species. Fortunately, due to the form of pdf's, integrals involving species and P_Q can be evaluated analytically.[5] The integrals involving T and P_T were evaluated numerically and stored in look-up table form as a function of T and the variance of T ($<T''^2>$), as done by Gerlinger *et al.*[12]

The remaining issue with respect to the evaluation of Equ. (1) is the specification of the temperature variance and scalar energy. These quantities were evaluated using modeled evolution equations[8,13] derived from the species and energy equations and are given by,

$$\frac{D\overline{\rho}<g>}{Dt} = \frac{\partial}{\partial x_j}\left(\overline{\rho}\overline{\gamma}\left(\frac{\overline{\nu}}{\mathrm{Pr}}+\frac{\overline{\nu}_T}{\mathrm{Pr}_T}\right)\frac{\partial <g>}{\partial x_j}\right) + 2C_1\overline{\rho}\overline{\gamma}\frac{\overline{\nu}_T}{\mathrm{Pr}_T}\left(\frac{\partial <e>}{\partial x_j}\right)^2 - 2C_g\overline{\rho}<g>\frac{\varepsilon}{k} - 2(\overline{\gamma}-1)\overline{\rho}<g>\frac{\partial <u_j>}{\partial x_j} \tag{12}$$

$$\frac{D\overline{\rho}Q}{Dt} = \frac{\partial}{\partial x_j}\left(\overline{\rho}\left(\frac{\overline{\nu}}{Sc}+\frac{\overline{\nu}_T}{Sc_T}\right)\frac{\partial Q}{\partial x_j}\right) + 2C_2\overline{\rho}\frac{\overline{\nu}_T}{Sc_T}\sum_{k=1}^{K}\left(\frac{\partial <Y_k>}{\partial x_j}\right)^2 - 2C_Q\overline{\rho}Q\frac{\varepsilon}{k} + 2\sum_{k=1}^{K}\overline{\dot{w}_k Y_k''} \tag{13}$$

where e is the internal energy, $<g>$ is the internal energy variance, u_j is the velocity, γ is the ratio of specific heats and k and ε are the turbulent kinetic energy and energy dissipation rate. The coefficients ν, ν_T, Sc and Pr are the kinematic viscosity, turbulent eddy viscosity, and Schmidt and Prandtl numbers, respectively. The length scales of the temperature and species fluctuations were assumed to be proportional to the velocity length scale and specified in terms of the turbulent Schmidt and Prandtl numbers, Sc_T and Pr_T, respectively. The last term in Equ. (12) is a modeled

dilatation term resulting from compressibility effects.[8] The last term in Equ. (13) is a chemical source term which may be evaluated using the assumed pdf's as described by Gaffney *et al.*[5]

The temperature and the temperature variance were obtained from the mean internal energy, $<e>$, and its variance, $<g>$, following a procedure used by Baurle and Girimaji.[10] First, the temperature and species fluctuations were neglected in the definition of the mean internal energy so that the temperature may be evaluated in the usual manner by solving $< e > -\sum_{k=1}^{K} < Y_k >< e_k >= 0$. Second, to obtain $< T''^2 >$, the specific heat, c_v, was linearized about the mean temperature so that,

$$< T''^2 > \approx \frac{< g >}{\hat{c}_v^{\,2}} \tag{14}$$

where $\hat{c}_v = c_v(< T >, < Y_k >)$.

The dissipation coefficients C_g and C_Q in Equs. (12) and (13), respectively, were specified as $C_g = C_Q = 0.544$ by matching the modeled scalar decay rate to that obtained from the DNS results of Eswaran and Pope[14] and McMurtry, *et al*[15] for *forced* isotropic turbulence. The production coefficients in these equations were specified as $C_1 = 0.2$ and $C_2 = 0.5$ as will be discussed in a later section.

III. COMPUTATIONAL METHODOLOGY

The missile plume flowfields in this study were analyzed using CRAFT[16] which is a structured, finite-volume code that solves the compressible Navier-Stokes (NS) equations. The solver is fully implicit and uses Roe/TVD numerics for the inviscid fluxes and second-order central differencing for viscous and diffusive terms. CRAFT is sufficiently general to simulate finite-rate chemistry and multi-phase flows and includes standard polynomial curve fits for the thermodynamic properties. The code includes a variety of advanced turbulence model formulations.[17] However, in this study, only the standard compressibility corrected k-ε model was used. CRAFT also includes an implementation of the assumed pdf turbulence-chemistry interaction model described in the previous

section. The CRAFT code achieves good computational efficiency through a fully parallelized implementation of the flow solver using a combined shared and distributed memory (using MPI) data parallel model. Computational efficiency is also enhanced using a parabolized form of the NS flow solver (PNS) for parabolic/hyperbolic regions of the flow. This PNS solver includes a sub-stepping option to allow for axial grid refinement in regions where flow properties change rapidly.

Radiation calculations were decoupled from the flowfield simulations and were carried out as described by Ludwig *et al.*[18] and Nelson[19]. Within this approach, radiation transport equations were solved using a band model for the gas phase absorption/emission. The calculations for the present study used a wide band pass to encompass emissions from *OH*, *CO*, CO_2 and H_2O. Total radiation intensity predictions were also made using a field of view large enough to encompass the entire plume.

IV. ROCKET PLUME SIMULATIONS

The simulations considered in this study were carried out for a generic axisymmetric amine booster described in detail by Calhoon[4]. The exhaust nozzle was assumed to have an area ratio of 10 and protrude aft of the booster base. The entire missile body-base-plume was simulated using CRAFT's NS and PNS solvers. The elliptic regions along the body and in the base region were computed using the NS solver. The hyperbolic plume flow was calculated using the PNS option. Each axisymmetric solution used *49,000* grid points to resolve the body-base region and *700,000* points for the plume region. Each grid, both body-base and plume, was manually adapted around regions with high gradients to ensure proper resolution of the flow features.

The inflow boundary conditions at the engine nozzle exit plane were specified from a separate nozzle flow calculation described in detail by Calhoon.[4] A standard 9 species – 10 reaction step mechanism[4] for H_2/CO oxidation was used for this calculation as well as for the plume simulations. For this nozzle simulation, the flow was fairly uniform across the exit, except within

the boundary layer region along the wall. The nozzle core temperature was ~ *1330 K*. The fuel-rich conditions of the engine were evident from an excess of *CO* and some H_2 in the core with O_2 virtually depleted. This nozzle solution was assumed to be invariant with respect to altitude and was used for all the body-base-plume calculations. This solution, however, did not account for turbulence-chemistry interactions within the nozzle. At this inflow, the temperature intensity was specified as 5% while the turbulent scalar energy was specified as 0%.

V. RESULTS AND DISCUSSION

The body-base and plume flowfields were calculated at three altitudes (*25 km*, *30 km* and *35 km*) both with and without the pdf model described earlier. These altitudes were selected because they span the afterburning shutdown regime for this generic booster, given an assumed trajectory profile.[4] The Reynolds and Mach numbers based on freestream conditions and the body radius were $Re_\infty = 4x10^6$, $2x10^6$ and $1x10^6$ and $M_\infty = 2.6$, *3.2* and *3.9* for the altitudes of *25*, *30* and *35 km*, respectively.

Plume simulations were carried out at these three altitudes for three different levels of modeling. The first assumed turbulence-chemistry interactions to be negligible. This approach was termed the 'laminar' reaction rate model. The second model included turbulence-chemistry interactions via the temperature pdf only, while the third approach included both the temperature and species pdf's. These three levels of modeling were considered not only to assess the effect of turbulence-chemistry interactions on missile plume afterburning shutdown, but also to assess the effectiveness of the different aspects of the assumed pdf model itself. For the pdf cases, the absolute temperature limits, T_0 and T_1, required to evaluate the pdf temperature limits, T_{min} and T_{max}, in Equ. (8) were specified as follows. With the freestream temperatures for the specified flight conditions ranging from *222* to *239 K*, the absolute minimum temperature was specified as $T_0 = 210$ *K*. The maximum absolute temperature, T_1, was specified as *2800 K* which corresponded to the maximum

temperature in the boundary layer along the nozzle wall.[4] With these absolute temperatures, the maximum realizable temperature intensity was $\sqrt{<T''^2>}/<T>\sim 1.6$, which corresponds to the condition when freestream and nozzle boundary layer fluid co-exist in an unmixed state.

As described by Calhoon,[4] the altitude conditions of *25*, *30* and *35 km* characterize the afterburning shutdown regime of the present generic booster system when simulated using the 'laminar' reaction rate model. For this model, the plume at *25 km* is burning vigorously, while at *30 km* it has progressed deep into the shutdown regime. At *35 km* the plume flame is almost completely extinguished. Application of the assumed pdf model to these flight conditions was found to have a substantial impact on the afterburning characteristics of this system. For example, Fig. 2 presents contour plots of temperature and CO_2 mole fraction at *30 km* for both the laminar rate and temperature pdf models. Simulations using both the temperature and species pdf will be discussed later. From this figure, the plume is seen to rapidly expand due to the highly underexpanded condition at the nozzle exit. The plume barrel shock is clearly evident in the temperature field along with its subsequent reflection off of the axis of symmetry and its interaction with the plume shear layer. Further downstream a series of weaker reflections persist until the plume shear layer merges with the axis. For the laminar rate case, plume ignition is delayed downstream until approximately three times the distance between the exit plane and the barrel shock reflection point. This is evident from the figure by the delay in the rise of CO_2 in the plume shear layer. This ignition delay also results in a long delay in the plume shear layer temperature rise. For the temperature pdf case, however, it is clear the model has a significant impact on the combustion processes occurring within the plume. For the pdf case, ignition occurs close to the missile base as evidenced by the rapid rise in shear layer CO_2. Further downstream, the plume vigorously afterburns resulting in higher plume temperatures.

The enhanced burning realized for the temperature pdf model at this altitude was found for the other altitudes as well. Fig. 3 presents a comparison of the laminar and temperature pdf rate model predicted mean temperatures along the plume axis for the three altitudes. In this figure the axial coordinate has been scaled by x_{refl}. This length scale is the distance between the nozzle exit plane and the barrel shock reflection point at the axis of symmetry. This reference length was found to approximately scale the results with respect to altitude so that a fixed value of x/x_{refl} corresponds to the same relative location in the plume for each case.[4] From Fig. 3, the pdf model is seen to enhance afterburning at all altitudes as evidenced from the higher peak temperatures in the plume farfield. At *25 km,* when the laminar model is vigorously afterburning, the difference between the two models is relatively small. However, as altitude is increased and afterburning shuts down for the laminar model, the differences become more pronounced. At *35 km*, the pdf case is still afterburning while the laminar rate case is becoming extinguished resulting in a temperature difference of approximately *100 K* in the farfield plume. As altitude is increased, the pdf model shows a gradual migration of the ignition point further downstream consistent with the laminar rate model. However, the temperature pdf model has delayed the onset of afterburning shutdown significantly.

Gaffney, *et al.*[8], found temperature fluctuations to enhance chemical reactions and ignition for high speed H_2-*air* shear layer flames that were far from equilibrium. The same observation may be made here with regard to CO/H_2-*air* combustion occurring in these plume flows. For the present plume application, the laminar rate model produces plume flames that are far from equilibrium and on the edge of burnout. When the pdf model is applied, temperature fluctuations enhance product formation resulting in higher plume temperatures and a delay in afterburning shutdown. This may be seen in Figs. 4 and 5 which are plots of CO_2 mole fraction and temperature, respectively, at $x/x_{refl} = 3$ for each altitude. The transverse coordinate in these figures has been scaled by δ which is the location at which the N_2 mole fraction is 99% of its freestream value for the laminar rate cases.

From Fig. 4, the temperature pdf model is seen to enhance the formation of CO_2 for all altitudes except *25 km*. At this altitude the laminar rate model produces more CO_2 than the pdf model. However, the H_2O formation (not shown) at *25 km* is much greater for the pdf model, offsetting the lower CO_2 formation so that the pdf model produces higher peak temperatures for all altitudes (Fig. 5). The enhancement of the H_2O chain within the mechanism results in a large enhancement of OH for the pdf cases as well (Fig. 6). For the laminar rate cases, Fig. 4 shows a large drop in peak CO_2 at this streamwise location as afterburning shuts down and the plume ignition point moves further downstream. The pdf model shows a similar trend but to a lesser extent, indicating the plume is shutting down slower. Also, similar to Fig. 3, Fig. 5 shows the impact of the pdf model on the temperature field to increase with increasing altitude.

The large impact of the assumed pdf method on plume combustion processes results from the influence of temperature fluctuations on the evaluation of the mean chemical reaction rate. Fig. 7 presents a plot of the temperature fluctuation intensity as a function of altitude at $x/x_{refl} = 3$. The fluctuation levels are seen to be quite large at this streamwise station and increase in magnitude with increasing altitude. These large values are a result of the excitation of the plume shear layer at the point where the reflected barrel shock intersects the layer. The increasing magnitude of the fluctuations indicates the pdf model is becoming increasingly important with increasing altitude. Consequently, neglecting these fluctuations would be inappropriate, especially as afterburning shutdown is approached. The primary effect of the temperature pdf model is on the ignition process so that prior to shutdown the model is much less significant as seen for the *25 km* case.

From Fig. 7 the model predicts the temperature intensity to increase with increasing altitude. From Equ. (12), it is unclear what the source of this trend is. Fig. 8 presents a plot of the production, dissipation and dilatation terms of Equ. (12) at $x/x_{refl} = 3$ for each altitude. From this figure the magnitude of each term is found to be decreasing with increasing altitude. The dilatation term also

has both positive and negative values and is small compared to the production and dissipation terms. Consequently, the modeled compressibility term in Equ. (12) did not explicitly play a significant role in the evolution of the energy variance. However, compressibility effects are implicitly influencing Equ. (12) through k and ε that evolve from the compressibility corrected k-ε model used in the simulations. Fig. 9 presents the sum of the production, dissipation and dilatation terms in Equ. (12) at this same streamwise location. From this figure, the total source term contribution to Equ. (12) is found to be rapidly decreasing with increasing altitude. This indicates that the increasing temperature intensity fluctuations seen in Fig. 7 are a result of upstream influences and not a result of enhanced relative production within the shear layer. Examination of contour plots of turbulent kinetic energy and temperature intensity show the plume shear layer to be greatly influenced by the reflected barrel shock. This reflected shock (see Fig. 2) excites the shear layer causing the layer to thicken and it enhances the production of turbulence and temperature fluctuations. This trend is consistent with the work of Norris and Edwards,[20] who applied a much more general unsteady *large-eddy* simulation technique to compute high-speed reacting exhaust flows. This shock-shear layer interaction determines the turbulence and temperature fluctuation levels which feed into the evolving shear layer. This interaction is the apparent source of the trend observed in Fig. 7.

The large increase in plume temperatures for the temperature pdf simulations correspondingly results in a large increase in plume radiative emissions. Figs. 10 and 11 present comparisons of station radiation and total radiant intensity, respectively. From Fig. 10, the station radiation for the pdf model is seen to be significantly larger than for the laminar rate model. Burning for the pdf model at *35 km* is also evident while the laminar model is approaching extinction. The higher station radiation predictions in Fig. 10 produce significant differences in the total plume intensity as seen in Fig. 11. As noted earlier, the pdf model has a greater influence as altitude is increased. This trend is also very apparent in Fig. 11. This figure also shows the pdf model to delay

the onset of afterburning shutdown and cause the plume to burn to higher altitudes than for the laminar rate model. The pdf model also significantly changes the afterburning shutdown rate, slowing it over what is seen for the laminar rate model.

Though changing the magnitude of the emissions, the pdf model did not change the *character* of the shutdown event seen in Fig. 11. Both the laminar and pdf models show a gradual type shutdown behavior which is characteristic of a Damköhler number effect as described by Calhoon.[4] As demonstrated by Calhoon,[4] a strain rate induced extinction phenomenon may be the source of rapid afterburning shutdown behavior which has been observed for some missile systems. A strain rate extinction mechanism is a consequence of turbulence-chemistry interactions. However, an extinction mechanism is *not* modeled within the present assumed pdf formulation. Therefore, the assumed pdf model cannot capture such a phenomenon.

As mentioned in Sec. II., the coefficients C_1 and C_2 on the production terms in Equs. (12) and (13) were specified as $C_1 = 0.2$ and $C_2 = 0.5$. The value C_2 was specified by optimizing the coefficient to match the scalar fluctuation data of Lockwood and Moneib[21] for a low speed nonreacting jet. Applying the same optimization procedure for Equ. (12) resulted in a value of *0.343* for C_1. Figs. 12 and 13 present the sensitivity of the temperature and temperature intensity with respect to variations in C_1 at $x/x_{refl} = 3$ for the *30 km* case. From Fig. 13, the temperature intensity is seen to vary by ~ *50 %* over the range $0.1 \leq C_1 \leq 0.343$ while the peak temperature in Fig. 12 varies by only ~ *6 %*. For simulations with $C_1 = 0.343$, the temperature intensities were high enough to force the plume afterburning to be at a near equilibrium condition for each altitude. Under this condition, the normalized CO_2 and H_2O mole fractions were invariant with altitude and afterburning shutdown was not initiated within the *25* to *35 km* window of the simulations. This result was unrealistic for the generic booster under consideration. This also indicates that the low speed calibration is inappropriate for application to the high speed, highly compressible flows of the

present context. The present value of $C_1 = 0.2$ was selected because it was close to the calibrated value and allowed afterburning shutdown to be initiated within the *25* to *35 km* window, as expected. The lower value of $C_1 = 0.1$ showed the same trends for mean flow quantities as for the present value of $C_1 = 0.2$, but to a slightly lesser extent. The value selected here for C_1' was deemed appropriate since the objective of this study was to make an assessment of the potential impact of turbulence-chemistry interactions on exhaust plume simulations, and not to make quantitative predictions.

This adjustment of C_1 from the low speed calibrated value to the smaller value of *0.2* is also consistent with the recent large-eddy simulation (LES) study of Calhoon, *et al.*[22] In that study, LES was used to investigate the effect of compressibility on temperature fluctuations in planar shear layers. It was found that compressibility effects in the high speed flow regime substantially reduced temperature fluctuations compared with what was found for low speed flows. The reduction in magnitude of these fluctuations was also similar to what have been accomplished in Fig. 13 by changing C_1. This finding suggests that the modeled compressibility term in Equ. (12) is inaccurate due to the fact that it made little contribution to the evolution of the energy variance as seen in Fig. 8. This reduction of C_1 has in some sense crudely represented the effects of compressibility as found by Calhoon, *et al.*[22] However, to resolve this issue will require the development of an accurate compressibility correction for Equ. (12) using LES or experimental data. In addition, a more advanced formulation may be required that includes a length scale equation for the temperature fluctuations.[23]

To investigate the effect of species fluctuations, Fig. 14 presents a comparison of the mean temperature at $x/x_{refl} = 3$ calculated using the temperature pdf only model and the full temperature and species pdf formulation described in Sec. II. From the figure it is apparent that the full temperature-species pdf formulation produced virtually identical results to the temperature pdf only

model. This was found to be true for the other flow variables as well. The ineffectiveness of the assumed *species* pdf model to significantly change the results can be traced to the prediction of the scalar energy, Q, from Equ. (13). Fig. 15 presents a plot of Q across the plume shear layer at $x/x_{refl} = 3$ calculated using Equ. (13) both *with* and *without* the chemical source term at *30 km*. Including the chemical source term causes Q to be driven to small values effectively turning off the species pdf model, producing the same result as for the temperature pdf only model. Eliminating this source term from Equ. (13) produces large values of scalar energy as seen in the figure. This chemical source term was found to be dissipative and to destroy the scalar energy and drive it to small values. Baurle, *et al.*[24], observed the same behavior for a high speed H_2-*air* flame. In another publication, Baurle, *et al.*[25], also compared predictions of this source term using the assumed pdf model and a more comprehensive pdf evolution equation model for the same jet flame. This comparison showed the predictions of this term to generally be of opposite sign and to be different in magnitude by a factor of five. The present results support the assertion of Baurle, *et al.*[25], that the present form of the species pdf, P_Q, is incapable of computing the higher order moments required to evaluate the Q chemical source term with any reasonable degree of accuracy. This also casts doubt on the assumed *species* pdf model's accuracy for computing the mean species reaction rate (Equation (1)) which often contains higher moments as well. This deficiency of the model is likely the source of the ineffectiveness of the assumed species pdf formulation.

As a final topic, to demonstrate the adequacy of the computational grid resolution, Figs. 16 and 17 present plots of the temperature and CO_2 mole fraction at two locations in the plume for each altitude condition. Shown in these figures are results for the plume solutions on the original (fine) grid and a coarse grid with half as many points in each coordinate direction. As seen in Figs. 16 and 17, the results are virtually identical, indicating that the original grids adequately resolved the flowfields.

VI. CONCLUSIONS

A computational study was undertaken to assess the impact of turbulence-chemistry interactions on the afterburning and afterburning shutdown characteristics of a generic amine booster. Turbulence-chemistry interactions were accounted for using an assumed probability density function based method. Analysis of the simulation results including the model led to the following conclusions:

1) Turbulence-chemistry interactions modeled using the assumed pdf method were found to be a first order effect and have a large impact on plume signatures as afterburning shutdown was approached. The pdf model enhanced plume afterburning and delayed the onset of shutdown causing the plume to burn to higher altitudes than when the model was not included. However, the pdf model did not change the *character* of the shutdown event. The model produced a gradual type of shutdown behavior characteristic of a Damköhler number shutdown mechanism (Calhoon, 2000).[4] The model does not account for the rapid shutdown phenomenon identified by Calhoon.[4]

2) The assumed pdf model was found to become increasingly important as altitude increased. This resulted from the increasing trend of temperature fluctuations within the shear layer. This trend was found to be a result of shock-shear layer interactions within the plume.

3) The calibration constant on the production term in the energy variance equation obtained from optimization using low speed jet data was found to be inapplicable to high speed plume flows. This low speed calibration produced excessively high temperature fluctuations that resulted in unrealistic results. Lower values of the coefficient produced realistic results and demonstrated the importance of turbulence-chemistry interactions within plume flows. A recent LES study[22] suggests that the source of the difficulty is the lack of a credible compressibility correction within the energy variance equations. Consequently, a reduction in the production calibration constant was required to bring the modeled scalar fluctuation statistics in line with LES data. This issue highlights the need

for a rigorous validation of the energy variance equation for high speed flows before quantitative predictions can be made.

4) The species fluctuation aspect of the assumed pdf formulation was found to be ineffective in the present plume flows. Apparent inaccuracies in the evaluation of the chemical source term in the scalar energy equation resulted in the model turning itself off. This same trend has been observed by other investigators and suggests that a reformulation of the species fluctuation aspect of the model is warranted.

VII. ACKNOWLEDGEMENTS

The authors gratefully acknowledge the support of Tom Smith and Jay Levine of the Air Force Research Laboratory, Edwards AFB, CA, and the Missile Defense Agency. The authors also gratefully acknowledge the help of Alan Kawasaki of ERC, Inc., Edwards AFB, CA in carrying out the radiation calculations.

VIII. REFERENCES

[1]Reijasse, P. and Délery, J., "Investigation of the Flow Past the ARIANE 5 Launcher Afterbody," *Journal of Spacecraft and Rockets*, Vol. 31, No. 2, pp. 208–214, 1994.

[2]Kramer, O. G., "Evaluation of Thermal Radiation from the TITAN III Solid Rocket Motor Exhaust Plumes," AIAA Paper 70-842, Jun. 1970.

[3]Dash, S. M., Pearce, B. E., Pergament, H. S. and Fishburne, E. S., "Predictions of Rocket Plume Flowfields for Infrared Signature Studies," *Journal of Spacecraft and Rockets*, Vol. 17, No. 3, pp. 190–199, 1980.

[4]Calhoon, W. H., Jr., "Computational Assessment of Afterburning Cessation Mechanisms in Fuel Rich Rocket Exhaust Plumes," *Journal of Propulsion and Power,* Vol. 17, No. 1, 2001, pp. 111 – 119.

[5]Gaffney, R. L., Jr., White, J. A., Girimaji, S. S. and Drummond, J. P., "Modeling Turbulent and Species Fluctuations in Turbulent, Reacting Flow, " *Computing Systems in Engineering*, Vol. 5, No. 2, 1994, pp. 117–133.

[6]Hsu, A. T., Tsai, Y.-L. P. and Raju, M. S., "Probability Density Function Approach for Compressible Turbulent Reacting Flows," *AIAA Journal*, Vol. 32, No. 7, 1994, pp. 1407–1415.

[7]Delarue, B. J. and Pope, S. B., "Calculation of Subsonic and Supersonic Turbulent Reacting Mixing Layers Using Probability Density Function Methods," *Physics of Fluids*, Vol. 10, No. 2, 1988, pp. 487–498.

[8]Gaffney, R. L., Jr., White, J. A., Girimaji, S. S. and Drummond, J. P., "Modeling Turbulent/Chemistry Interactions Using Assumed PDF Methods," AIAA Paper 92-3638, July 1992.

[9]Pearce, B. E. and Varma, A. K., "Radiation-Turbulence Interaction in a Tactical Missile Exhaust Plume," AIAA Paper 81-1110, June 1981.

[10]Baurle, R. A. and Girimaji, S. S., "An Assumed PDF Turbulence-Chemistry Closure with Temperature-Composition Correlations," AIAA Paper 99-0928, Jan. 1999.

[11]Girimaji, S. S., "Assumed b-pdf Model for Turbulent Mixing: Validation and Extension to Multiple Scalar Mixing," *Combustion Science and Technology*, Vol. 78, 1991, pp. 177–196.

[12]Gerlinger, P., Brüggemann, D. and Möbus, H., "An Implicit Numerical Scheme for Turbulent Combustion Using an Assumed PDF Approach," AIAA Paper 99-3775, June 1999.

[13]Baurle, R. A., Alexopoulos, G. A. and Hassan, H. A., "Assumed Joint Probability Density Function Approach for Supersonic Turbulent Combustion," *Journal of Propulsion and Power,* Vol. 10, No. 4, 1994, pp. 473–484.

[14]Eswaran, V. and Pope, S. B., "Direct Numerical Simulations of the Turbulent Mixing of a Passive Scalar,", *Physics of Fluids*, Vol. 31, No. 3, 1988, pp. 506–520.

[15]McMurtry, P. A., Gansauge, T. C., Kerstein, A. R. and Kruger, S. K., "Linear Eddy Simulations of Mixing in a Homogeneous Turbulent Flow," *Physics of Fluids A*, Vol. 5, No. 4, 1993, pp. 1023–1034.

[16]Sinha, N., Dash, S. M., and Hosangadi, A., "Applications of an Implicit, Upwind NS Code, CRAFT, to Steady/Unsteady Reacting, Multi-Phase Jet/Plume Flowfields," AIAA Paper 92-0837, Jan. 1992.

[17]Kenzakowski, D. C., Papp, J., and Dash, S. M., "Evaluation of Advanced Turbulence Models and Variable Prandtl/Schmidt Number Methodology for Propulsive Flows," AIAA Paper 2000-0885, Jan. 2000.

[18]Ludwig, C. B., Malkmus, W., Walker, J., Slack, M., and Reed, R., "The Standard Infrared Radiation Model," AIAA Paper 81-1051, Jun. 1981.

[19]Nelson, H. F., "Evaluation of Rocket Plume Signature Uncertainties," *Journal of Spacecraft and Rockets*, Vol. 24, No. 6, 1987, pp. 546–551.

[20]Norris, J. W. and Edwards, J. R., "Large-Eddy Simulation of High-Speed, Turbulent Diffusion Flames with Detailed Chemistry," *AIAA Paper 97-0370*, Jan. 1997.

[21]Lockwood, F. C. and Moneib, H. A., "Fluctuating Temperature Measurements in a Heated Round Free Jet," *Combustion Science and Technology*, Vol. 22, 1980, pp. 63–81.

[22]Calhoon, W. H., Jr., Kannepalli, C., and Dash, S. M., "LES Studies of Scalar Fluctuations at High Convective Mach Numbers," Third AFOSR International Conference on Direct Numerical Simulation and Large Eddy Simulations, University of Texas at Arlington, Aug. 5-9, 2001.

[23]Chidambaram, N., Dash, S. M. and Kenzakowski, D. C., "Scalar Variance Transport in the Turbulence Modeling of Propulsive Jets," *Journal of Propulsion and Power,* Vol. 17, No. 1, 2001, pp. 79 – 84.

[24]Baurle, R. A., Alexopoulos, G. A. and Hassan, H. A., "Modeling of Supersonic Turbulent Combustion Using Assumed Probability Density Functions," *Journal of Propulsion and Power,* Vol. 10, No. 6, 1994, pp. 777–786.

[25]Baurle, R. A., Hsu, A. T. and Hassan, H. A., "Assumed and Evolution Probability Density Functions in Supersonic Turbulent Combustion Calculations," *Journal of Propulsion and Power,* Vol. 11, No. 6, 1995, pp. 1132–1138.

Fig. 1. Illustration of the behavior of plume total radiant intensity as a function of altitude, (a) afterburning regime, (b) afterburning shutdown regime, and (c) post-afterburning shutdown regime.

Fig. 2. Contours of (a) temperature and (b) CO_2 mole fraction at *30 km* for both the laminar rate (lam) and temperature pdf (t pdf) models. The nozzle exit plane is at the top and downstream is to the bottom. The transverse direction has been scaled by a factor of 5 for clarity.

Fig. 3. Comparison of laminar and temperature pdf rate model predictions of centerline mean temperature at *25*, *30* and *35 km* ($x = 0$ is at the engine nozzle exit plane).

Fig. 4. Prediction of transverse mean CO_2 mole fraction at $x/x_{refl} = 3$ as a function of altitude for the laminar rate and temperature pdf models.

Fig. 5. Prediction of transverse mean temperature at $x/x_{refl} = 3$ as a function of altitude for the laminar rate and temperature pdf models.

Fig. 6. Prediction of transverse mean *OH* mole fraction at $x/x_{refl} = 3$ as a function of altitude for the laminar rate and temperature pdf models.

Fig. 7. Temperature intensity predictions from the assumed pdf model as a function of altitude at $x/x_{refl} = 3$.

Fig. 8. Transverse variation of the production, dissipation and dilatation terms in Equ. (12) at $x/x_{refl} = 3$ as a function of altitude.

Fig. 9. Transverse variation of the sum total of the production, dissipation and dilatation terms in Equ. (12) at $x/x_{refl} = 3$ as a function of altitude.

Fig. 10. Source station radiation variation as a function of altitude at a 90 degree aspect angle.

Fig. 11. Comparison of laminar rate and temperature pdf model predictions of source total radiant intensity as a function of altitude at a 90 degree aspect angle.

Fig. 12. Sensitivity of mean temperature to the calibration constant C_1 in Equ. (12) at $x/x_{refl} = 3$ for *30 km*.

Fig. 13. Sensitivity of temperature intensity to the calibration constant C_1 in Equ. (12) at $x/x_{refl} = 3$ for *30 km*.

Fig. 14. Prediction of transverse mean temperature at $x/x_{refl} = 3$ as a function of altitude using the temperature pdf only (t pdf) and the temperature-species pdf (ty pdf) formulations.

Fig. 15. Prediction of scalar energy from Equ. (13) both with and without the chemical source term included at $x/x_{refl} = 3$ and *30 km*.

Fig. 16. Plume temperature profiles for the original (fine) and coarse grid solutions for the laminar rate case at $x^* = x/x_{refl} = 3$ and *9*.

Fig. 17. Plume CO_2 mole fraction profiles for the original (fine) and coarse grid solutions for the laminar rate case at $x^* = x/x_{refl} = 3$ and *9*.

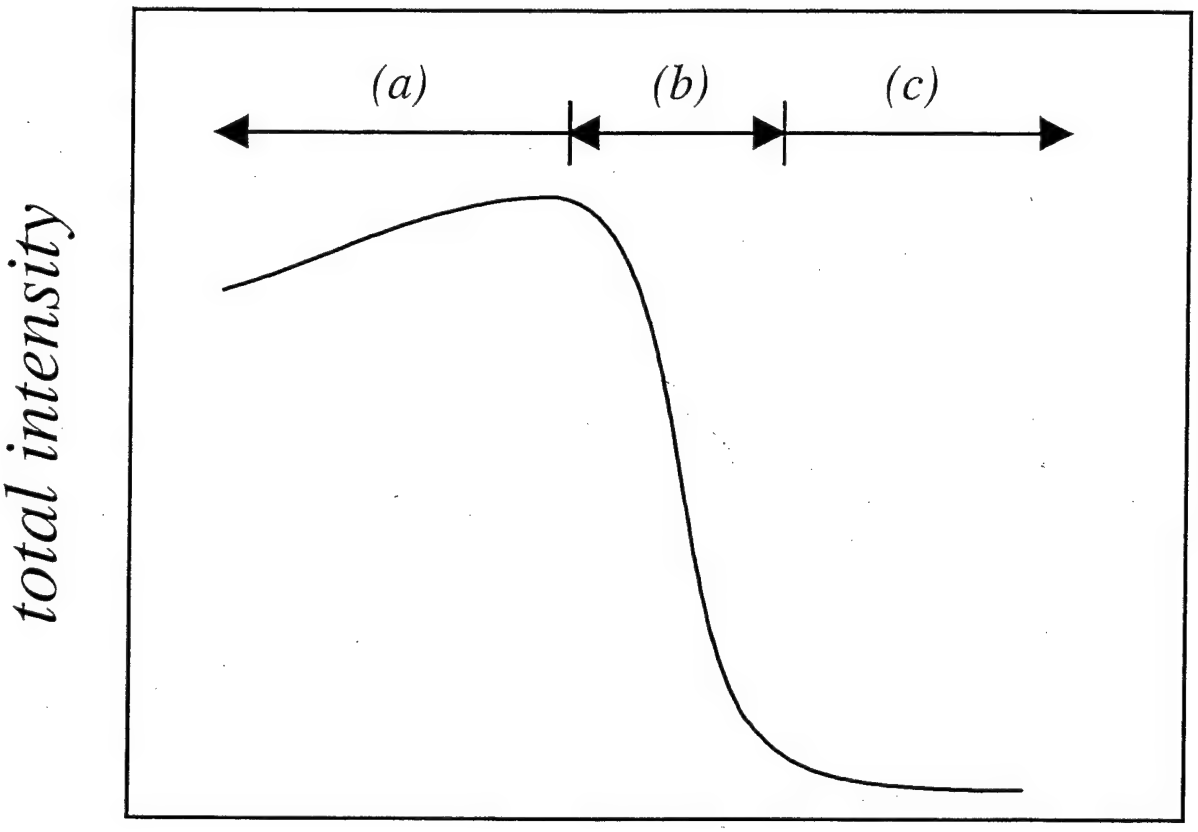

(1)

calhoon

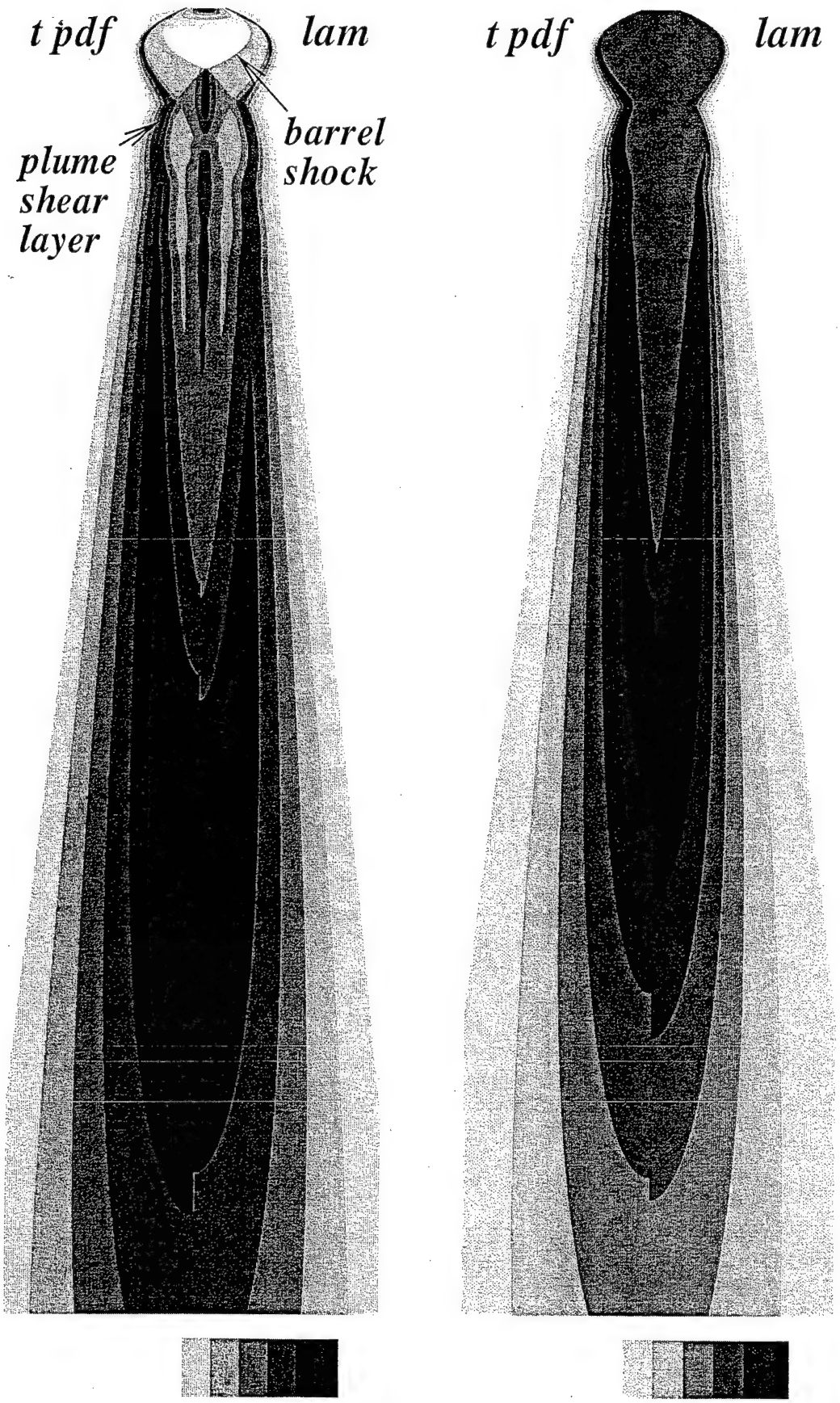
t pdf
lam
plume
shear
layer
barrel
shock
t pdf
lam
T (K): 300 1275
X_{CO2}: 0.0 0.1
(a)
(b)

(2)

Calhoon

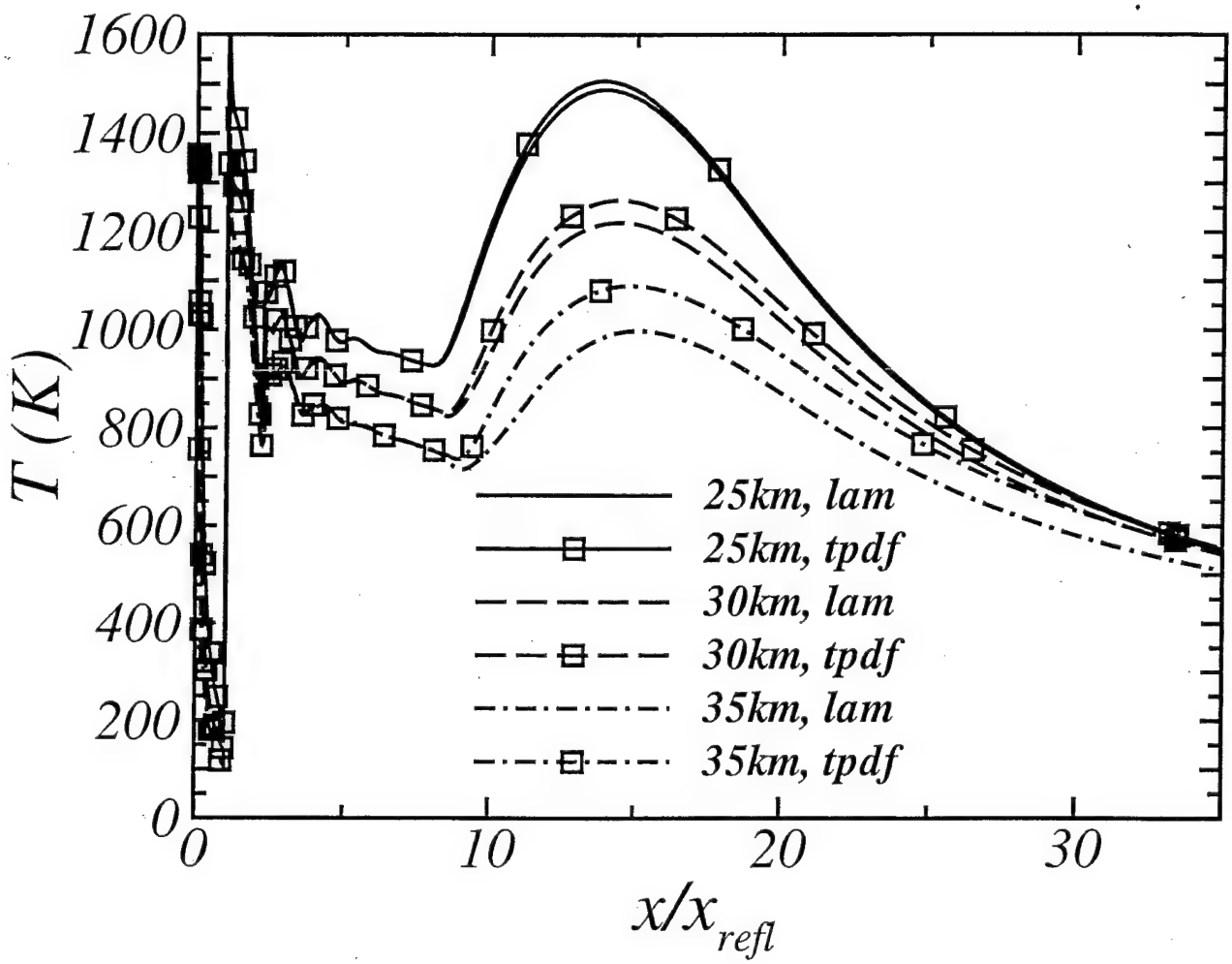
1600
1400
1200
1000
800
600
400
200
0
T (K)
0
10
20
30
x/x_refl
25km, lam
25km, tpdf
30km, lam
30km, tpdf
35km, lam
35km, tpdf

Calhoon

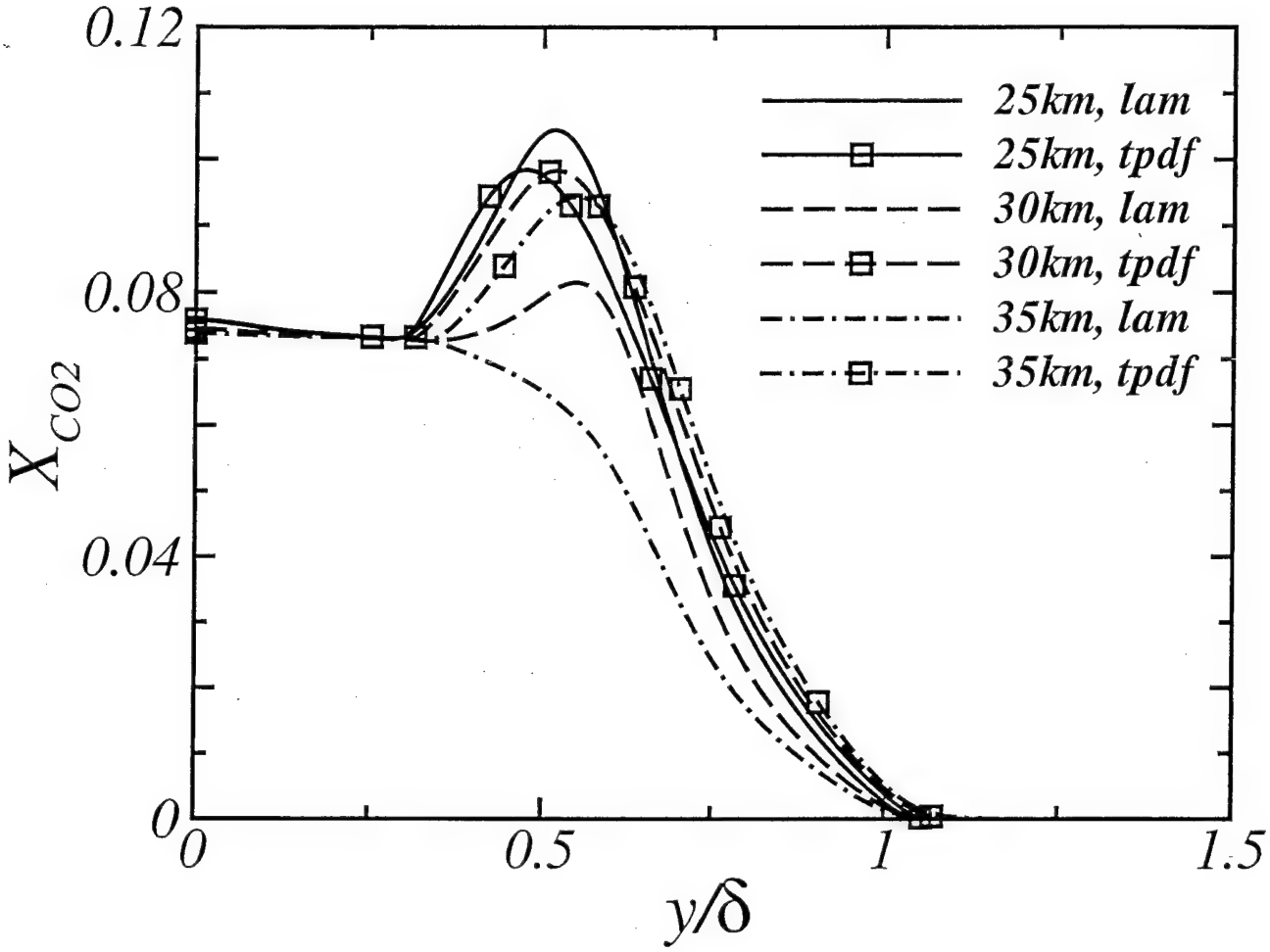
0.12
0.08
0.04
0
X_{CO2}
0
0.5
1
1.5
y/δ
25km, lam
25km, tpdf
30km, lam
30km, tpdf
35km, lam
35km, tpdf

calhoon

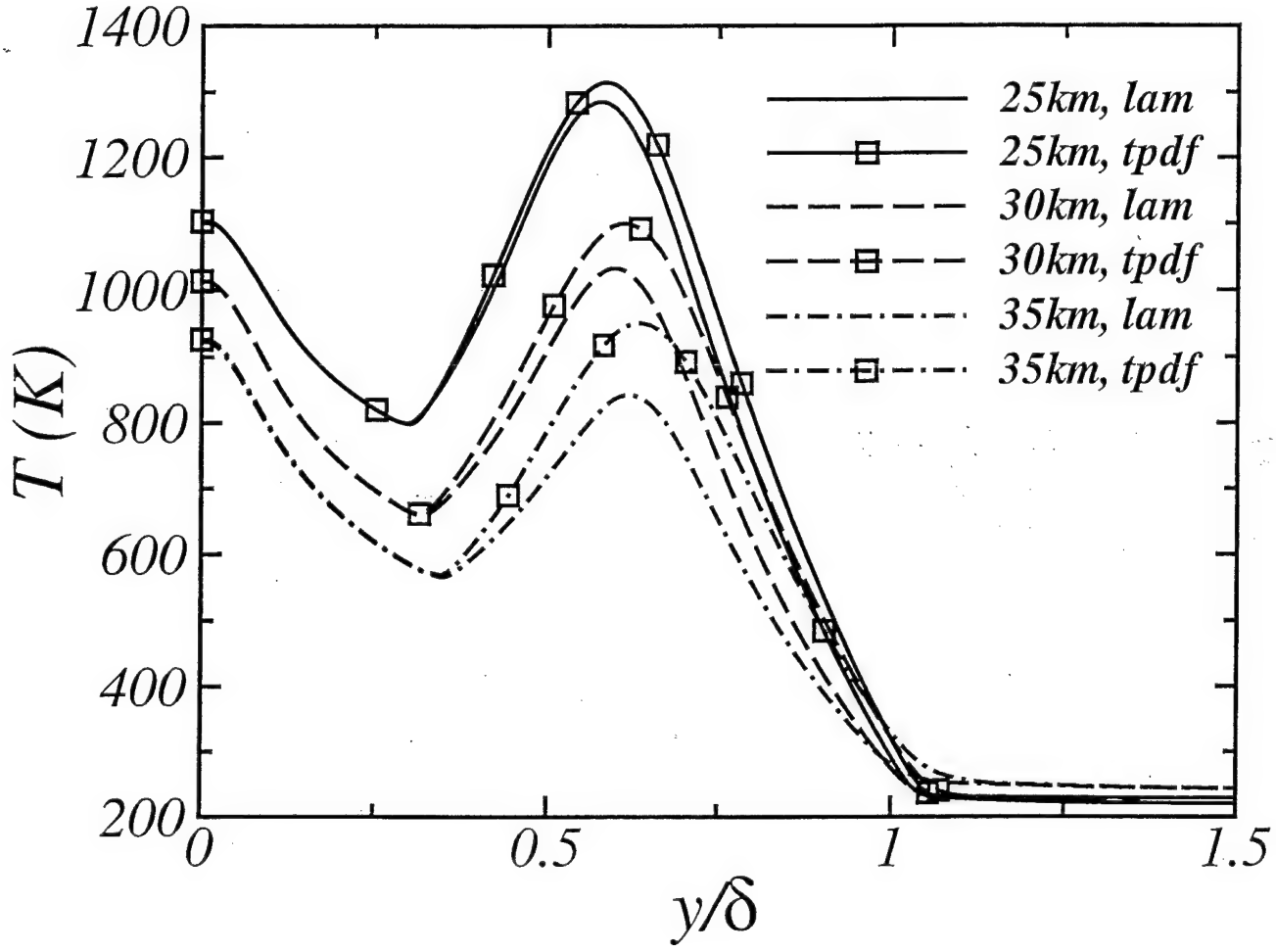
1400
1200
1000
800
600
400
200
T (K)
0
0.5
1
1.5
y/δ
25km, lam
25km, tpdf
30km, lam
30km, tpdf
35km, lam
35km, tpdf

Calhoon

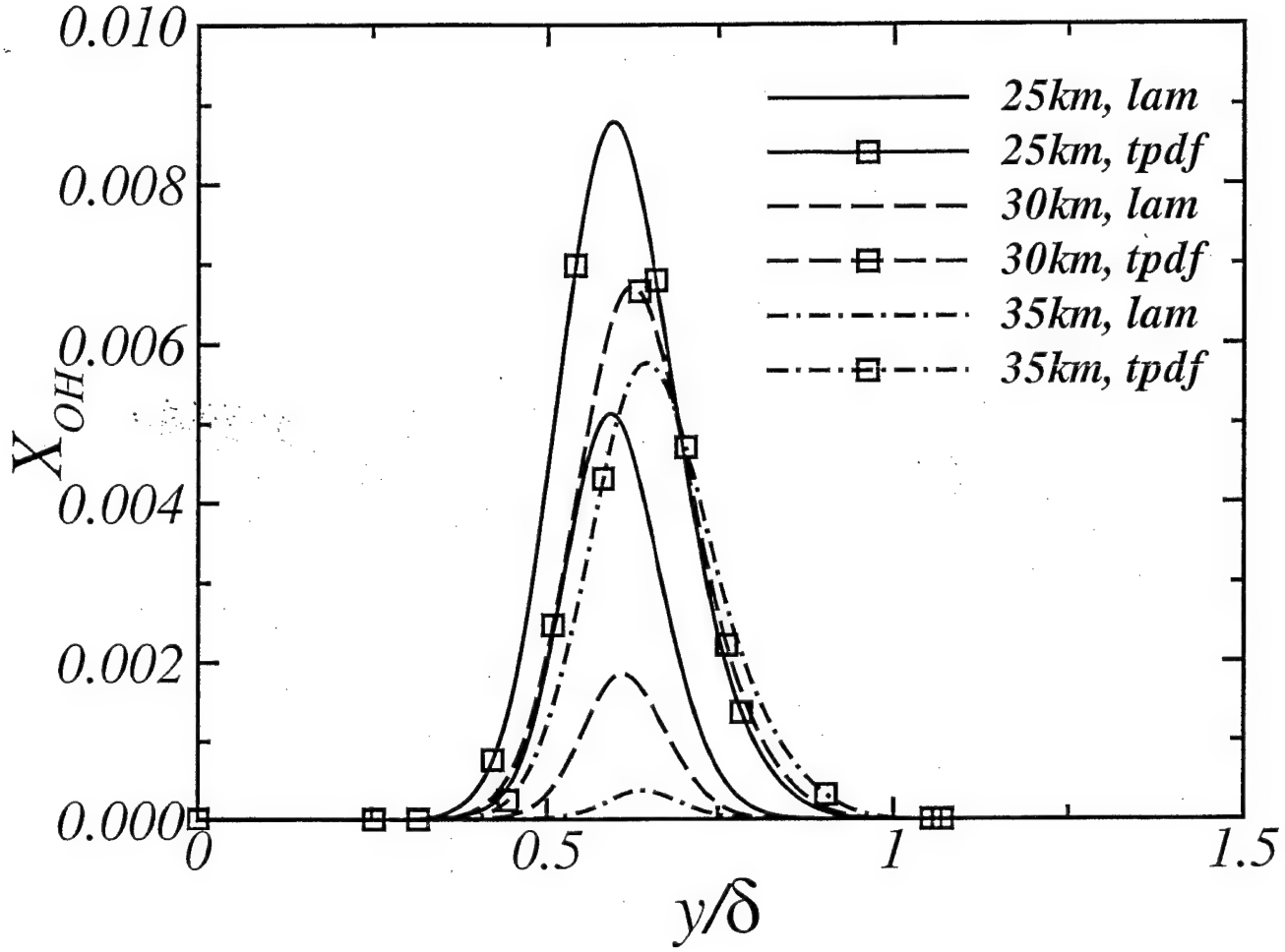
0.010
0.008
0.006
0.004
0.002
0.000
X_{OH}
0
0.5
1
1.5
y/δ
25km, lam
25km, tpdf
30km, lam
30km, tpdf
35km, lam
35km, tpdf

calhoon

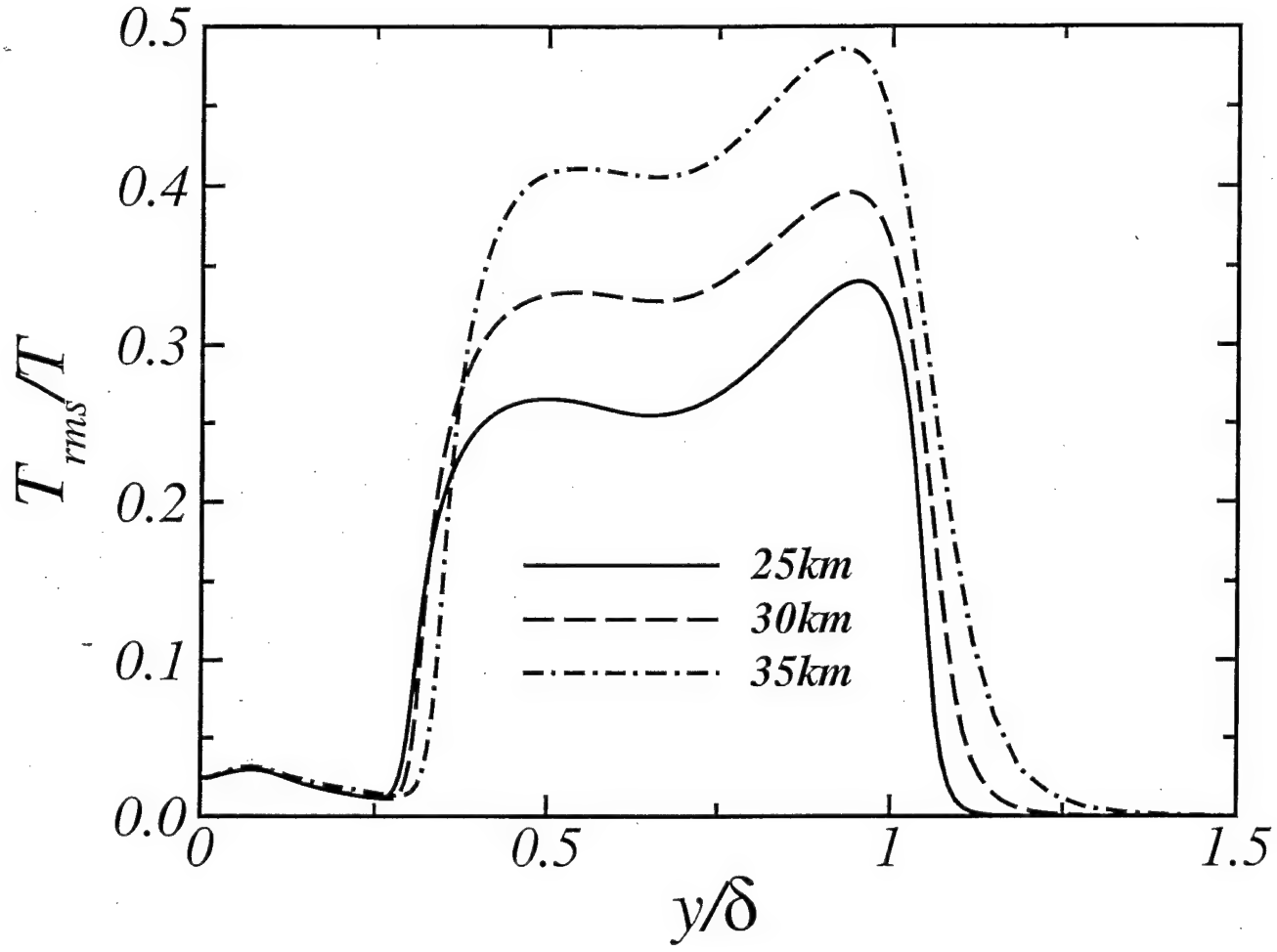

cahoon

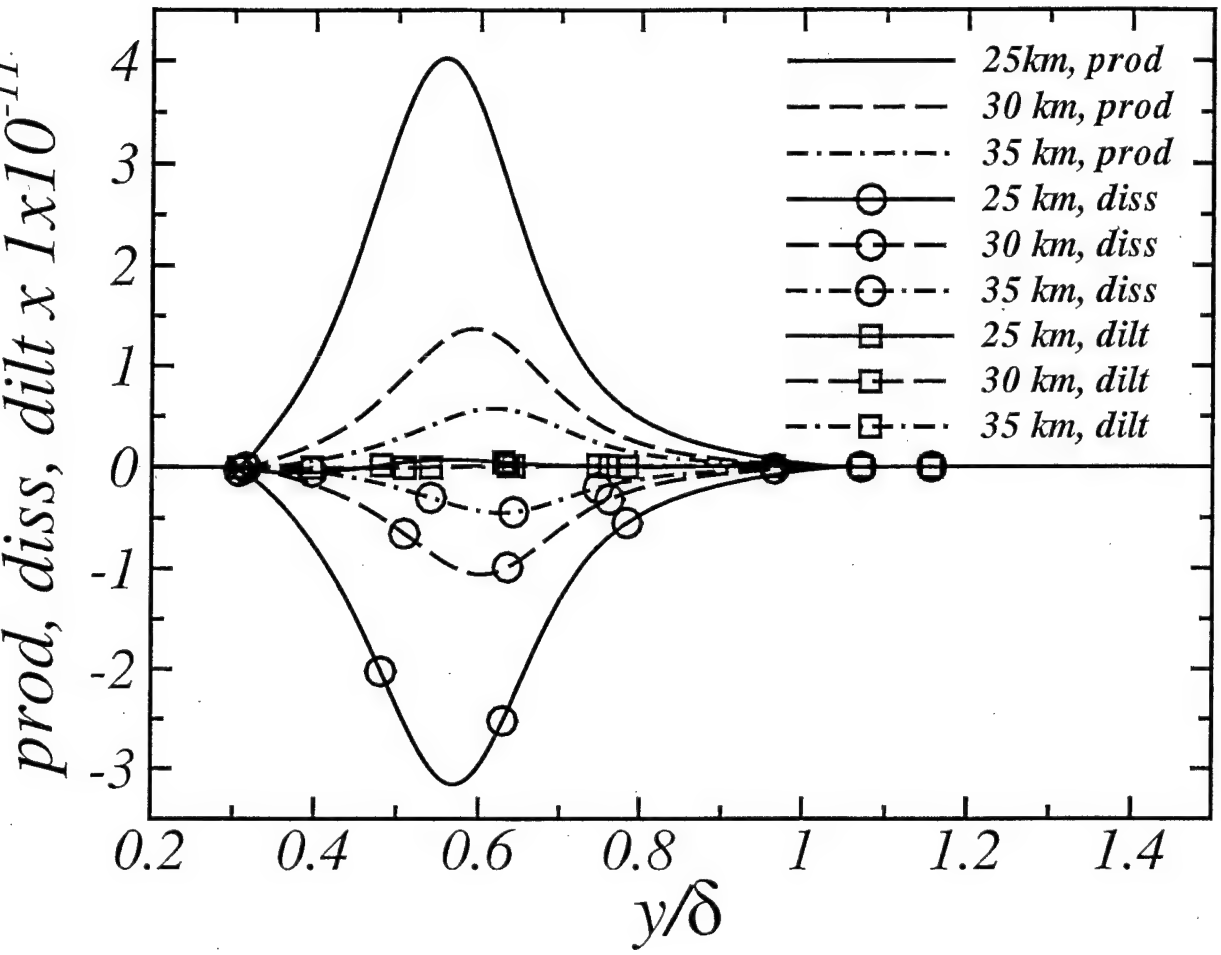
prod, diss, dilt x 1x10^-11
4
3
2
1
0
-1
-2
-3
0.2
0.4
0.6
0.8
1
1.2
1.4
y/δ
25km, prod
30 km, prod
35 km, prod
25 km, diss
30 km, diss
35 km, diss
25 km, dilt
30 km, dilt
35 km, dilt

calhoon

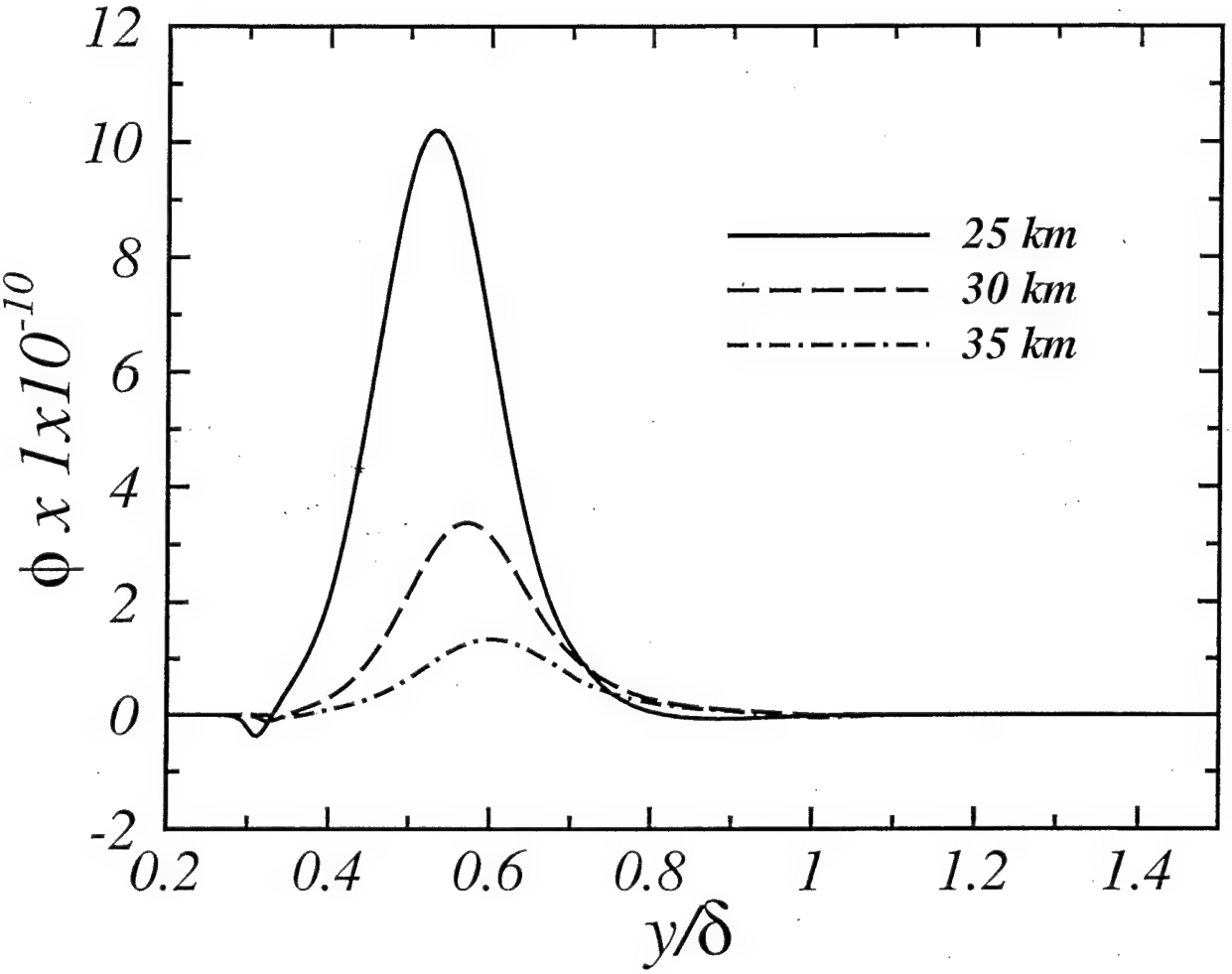

Calhoon

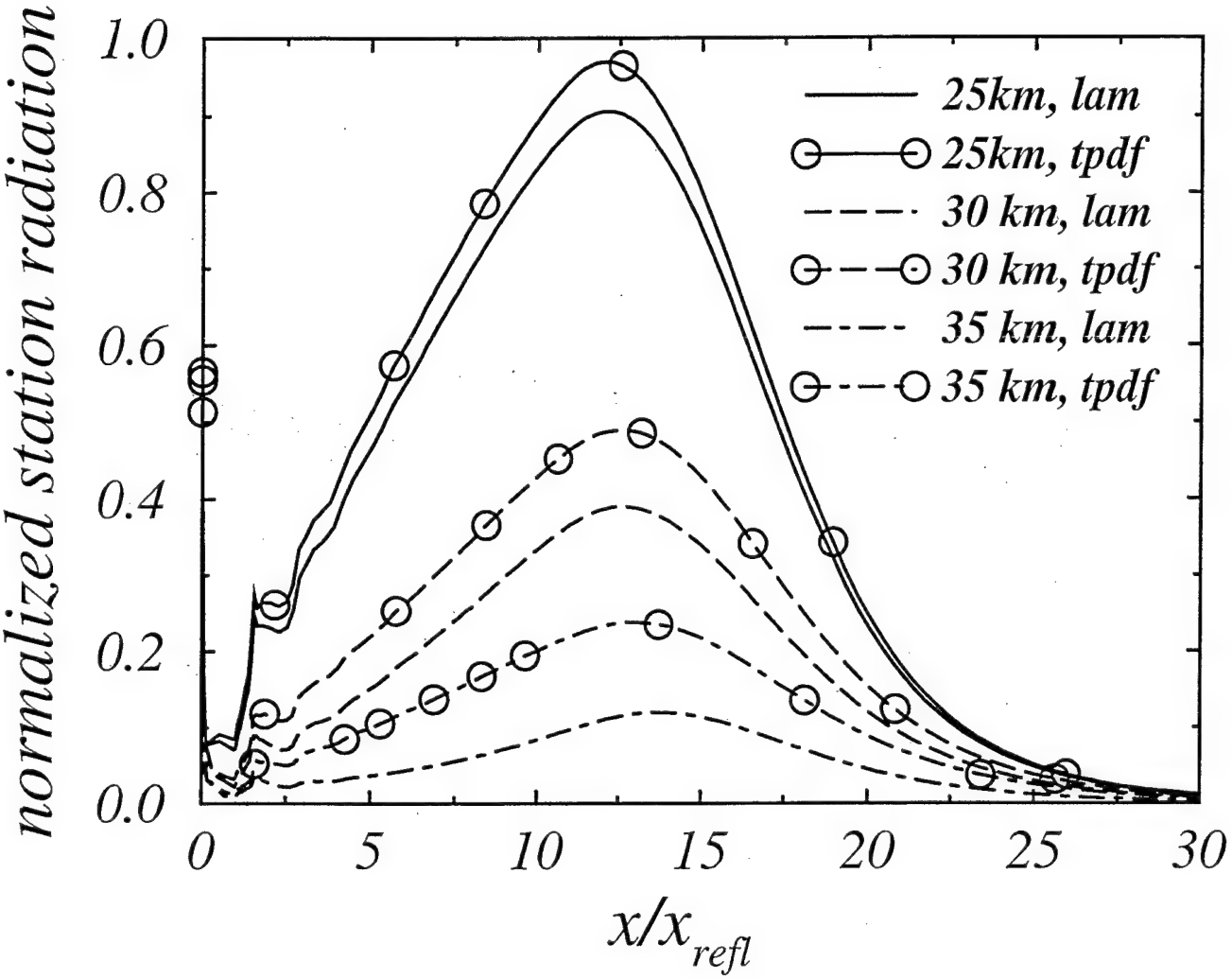
normalized station radiation
1.0
0.8
0.6
0.4
0.2
0.0
0
5
10
15
20
25
30
x/x_refl
25km, lam
25km, tpdf
30 km, lam
30 km, tpdf
35 km, lam
35 km, tpdf

calhoon

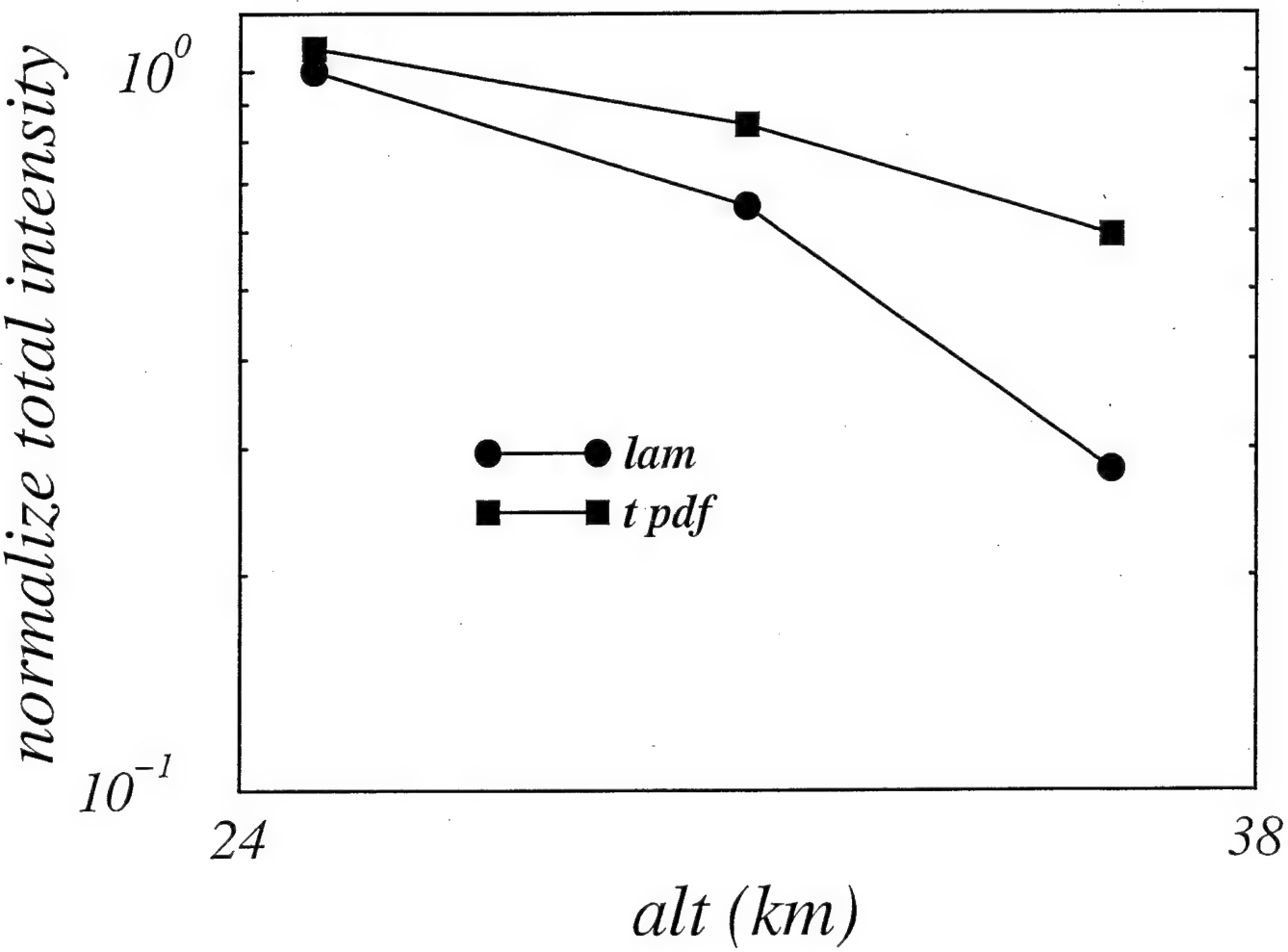

Calhoon

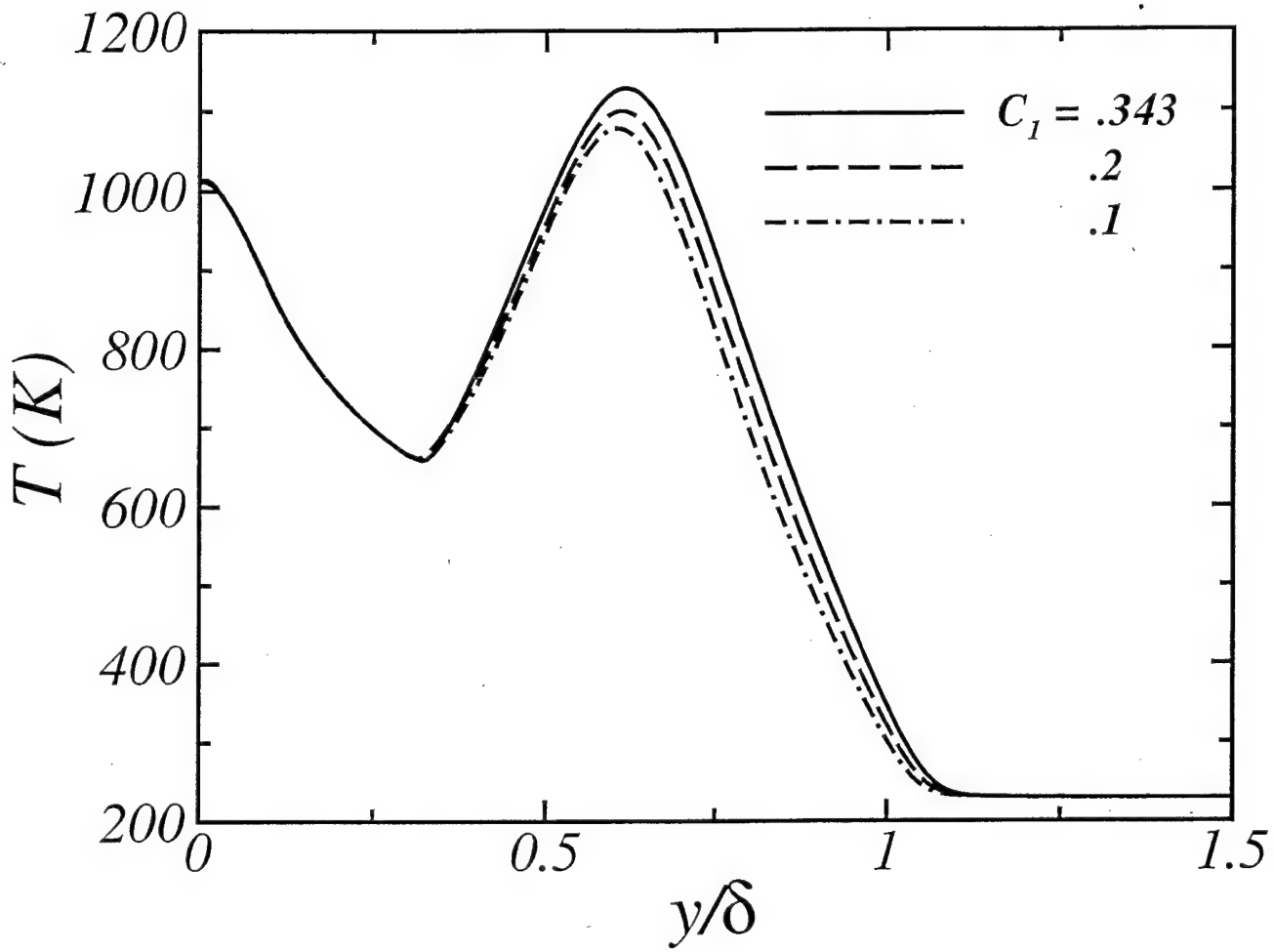

(12)

Calhoon

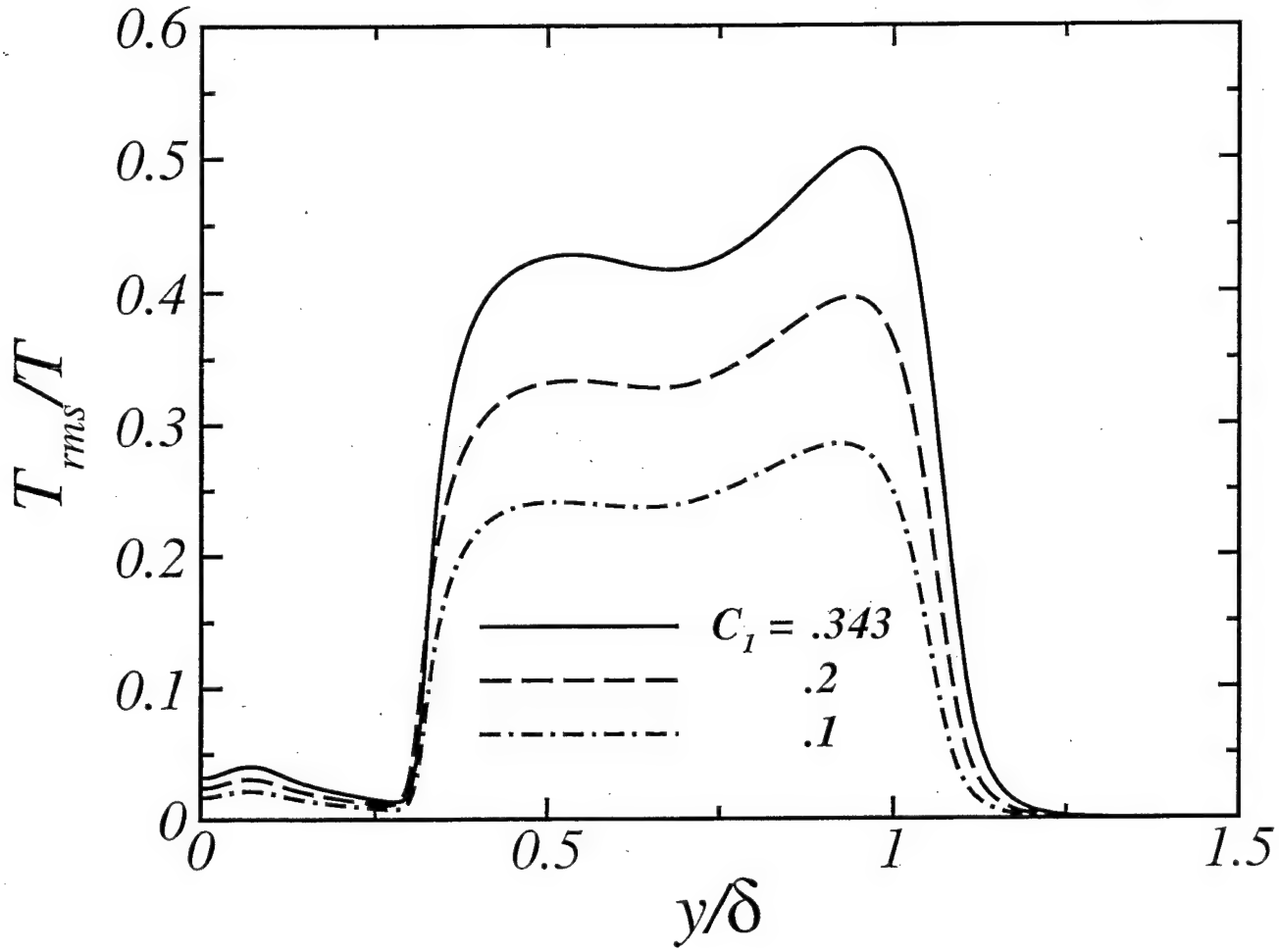

(13)

Galhoon

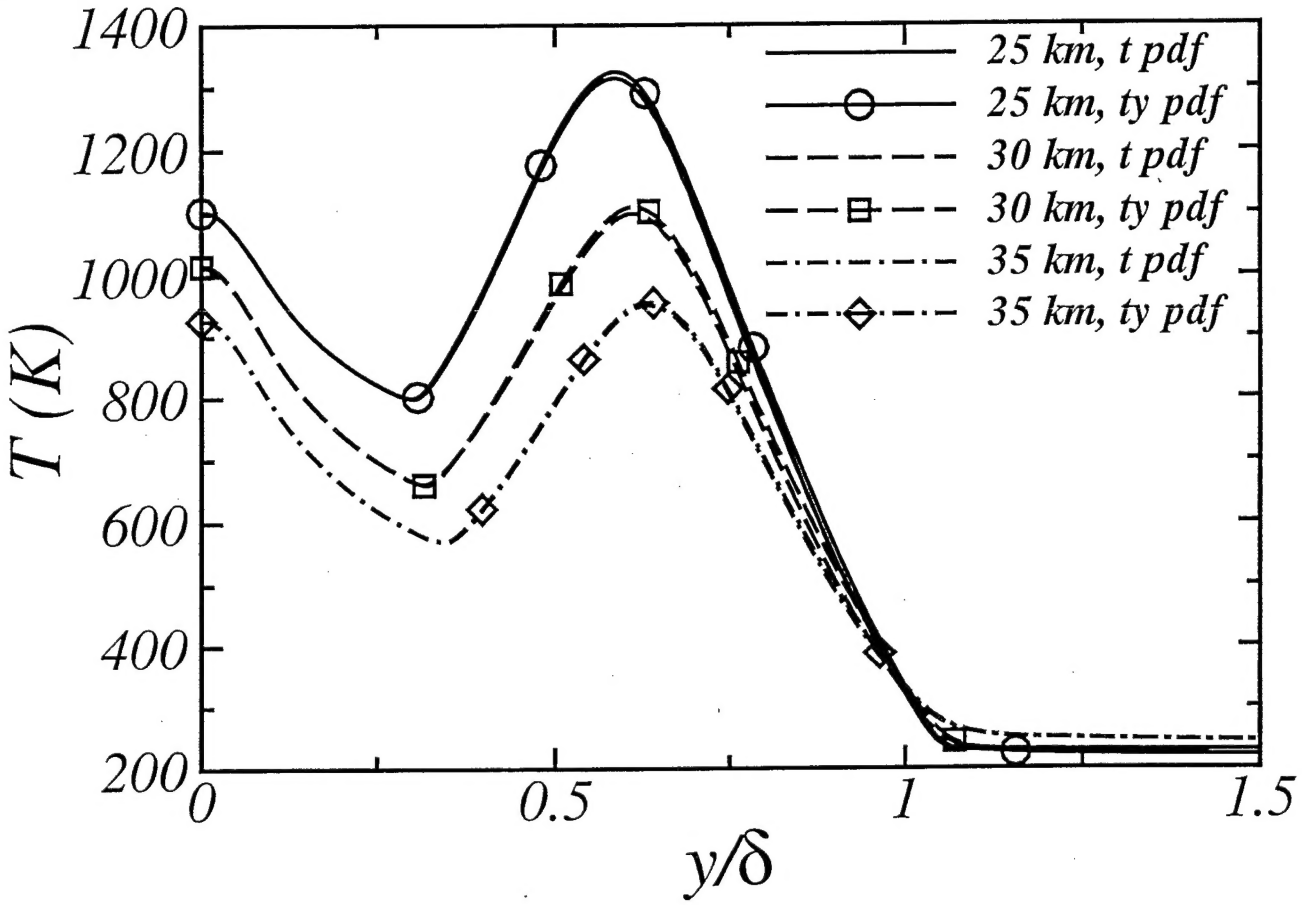
1400
1200
1000
800
600
400
200
T (K)
0
0.5
1
1.5
y/δ
25 km, t pdf
25 km, ty pdf
30 km, t pdf
30 km, ty pdf
35 km, t pdf
35 km, ty pdf

calhoon

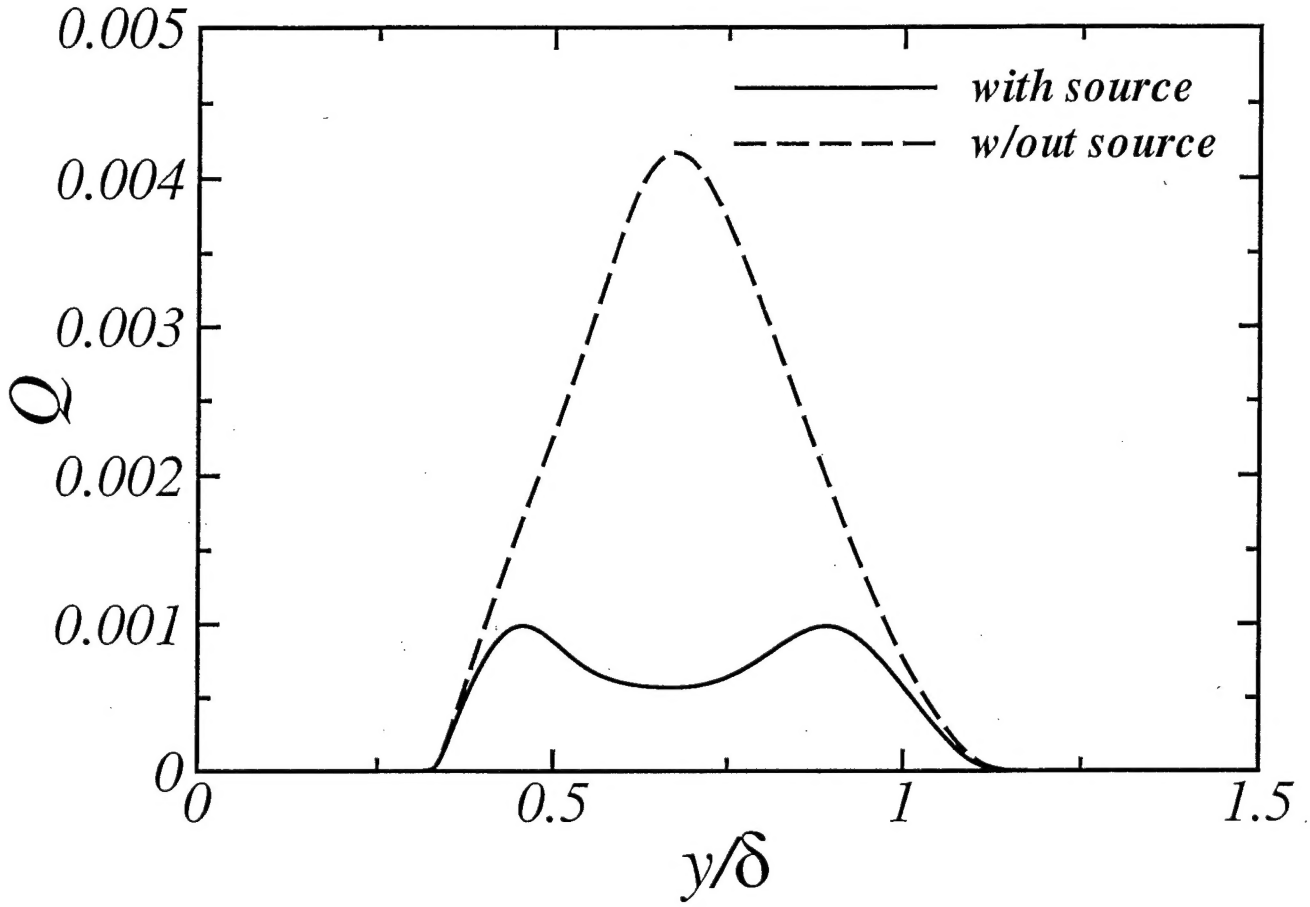
0.005
0.004
0.003
0.002
0.001
0
Q
0
0.5
1
1.5
y/δ
with source
w/out source

calhoon

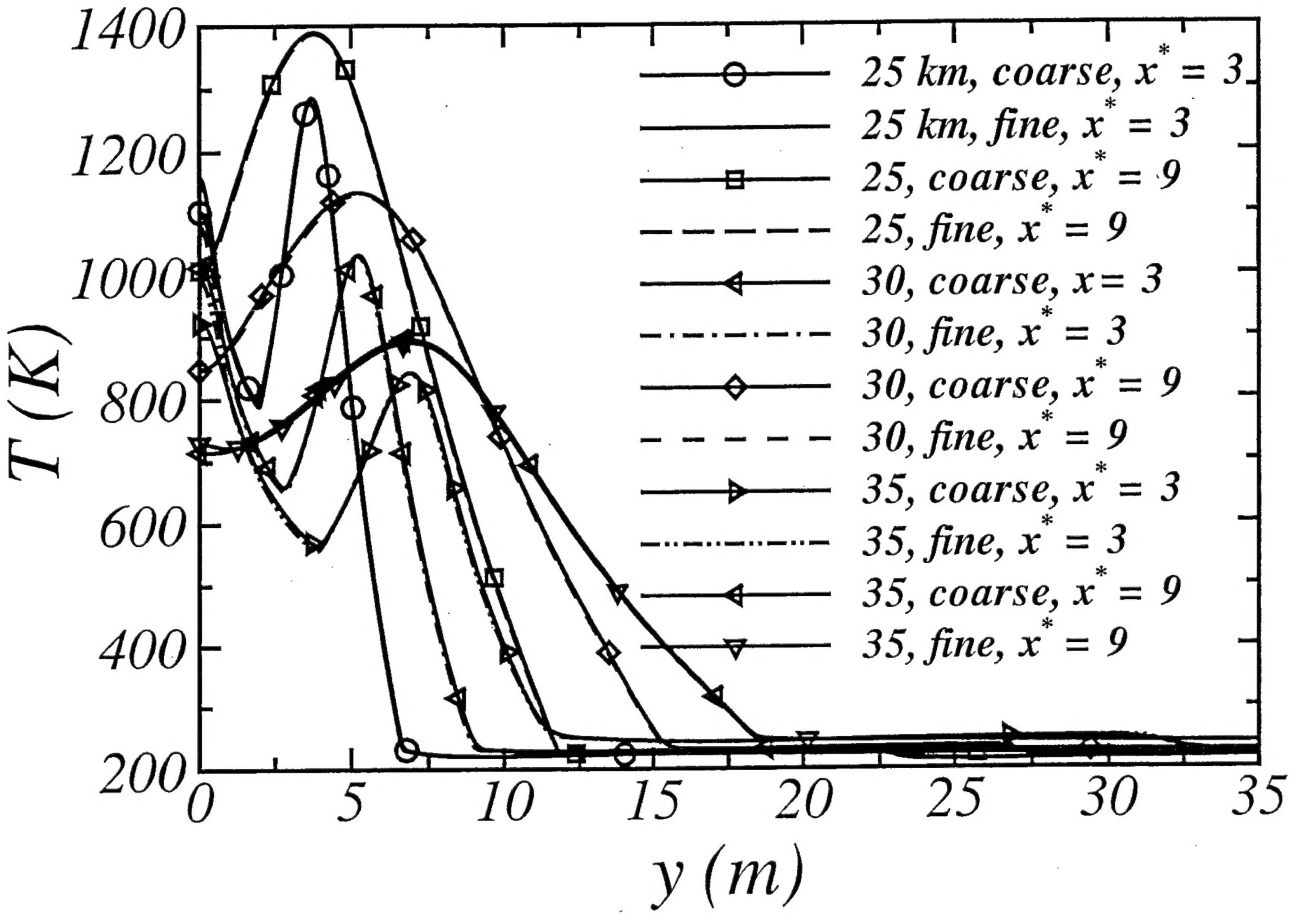
1400
1200
1000
800
600
400
200
T (K)
0
5
10
15
20
25
30
35
y (m)
25 km, coarse, x* = 3
25 km, fine, x* = 3
25, coarse, x* = 9
25, fine, x* = 9
30, coarse, x= 3
30, fine, x* = 3
30, coarse, x* = 9
30, fine, x* = 9
35, coarse, x* = 3
35, fine, x* = 3
35, coarse, x* = 9
35, fine, x* = 9

Calhoon

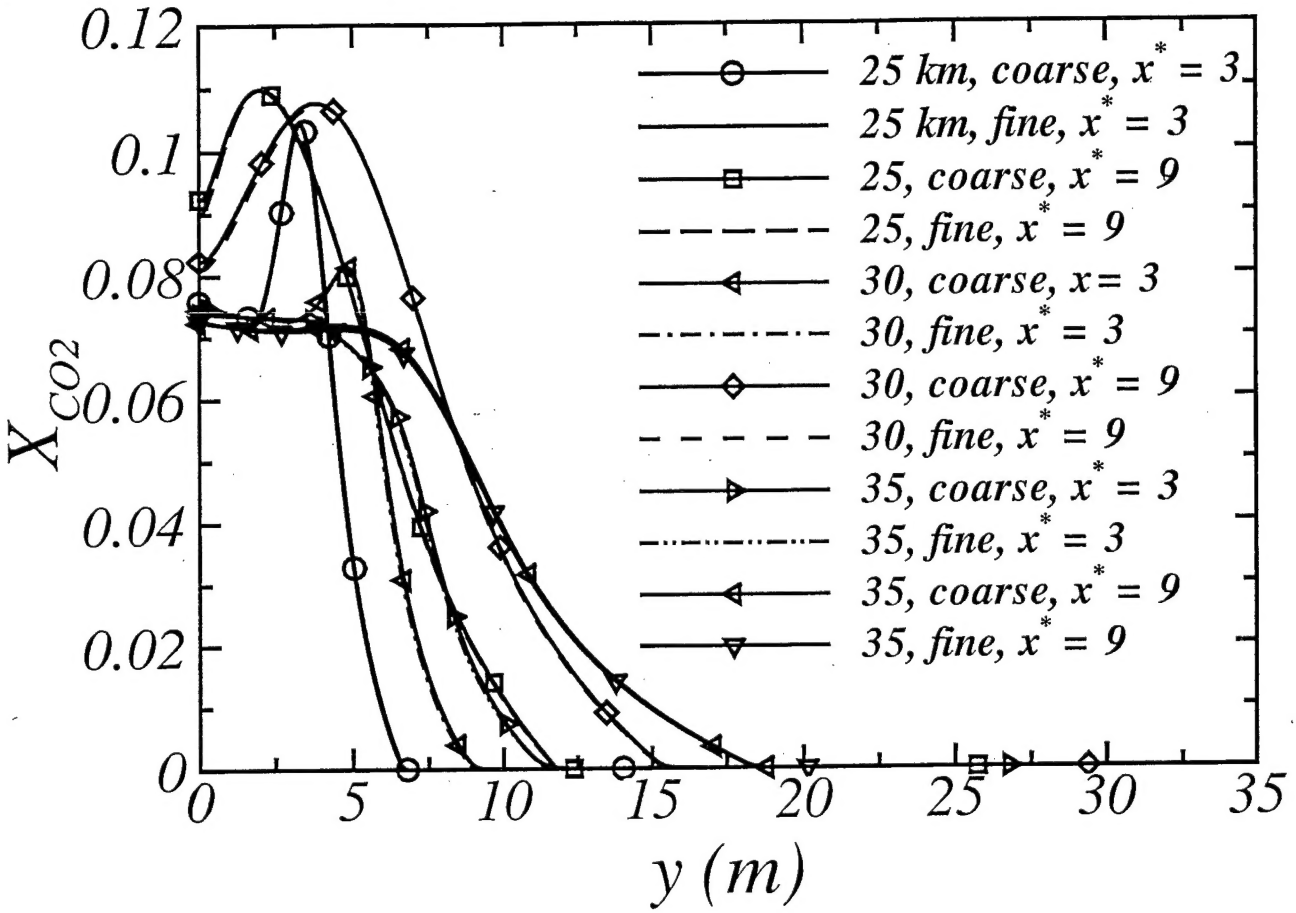
0.12
0.1
0.08
0.06
0.04
0.02
0
X_{CO2}
0
5
10
15
20
25
30
35
y (m)
25 km, coarse, x* = 3
25 km, fine, x* = 3
25, coarse, x* = 9
25, fine, x* = 9
30, coarse, x= 3
30, fine, x* = 3
30, coarse, x* = 9
30, fine, x* = 9
35, coarse, x* = 3
35, fine, x* = 9
35, coarse, x* = 9
35, fine, x* = 9

Calhoon